Review

Environmental Chemistry and Safety
DOI: 10.26599/ECS.2025.9600046
2025, 1, 9600046

Metal Sulfide-Based Catalysts for Advanced Oxidation Processes: Tailoring Strategies and Mechanistic Insights for Organic Pollutant Removal

Fei-Qin Bian[1,2], Ghulam Hassan Abbasi[3], Hong Chen[1*], and Lin-Dong Liu[1,2*]

[1]Interdisciplinary Research Centre for Agriculture Green Development in Yangtze River Basin, International S & T Cooperation Base on Water Environmental Monitoring and Simulation in TGR Region, Department of Environmental Sciences and Engineering, College of Resources and Environment, Southwest University, Chongqing 400716, China

[2]Yibin Academy of Southwest University, Sichuan 644005, China

[3]Institute of Agro-Industry & Environment, Faculty of Agriculture & Environment, The Islamia University of Bahawalpur, Pakistan

Abstract: Metal sulfides are abundant in nature. They also have excellent catalytic qualities and tunable electronic structures. These characteristics make them extremely attractive materials advanced oxidation processes (AOPs) in wastewater treatment. In this review, the relationship between structure and property in monometallic and bimetallic sulfides is examined in detail. The key point is to introduce their working mode - activating peroxymonosulfate (PMS), peroxydisulfate (PDS) and hydrogen peroxide to generate reactive oxygen species. The key methods for improving catalytic performance were elaborated in detail. This includes the rational design of bimetallic sulfides, introduction of sulfur vacancies, non-metal doping and in-situ regeneration techniques. These methods can adjust the electronic configuration, expose active sites and accelerate the metal redox cycling effectively. This greatly enhances the degradation efficiency and maintains the stability of the catalyst. This review also studies the environmental factors that affect catalytic performance. It points out future directions for developing metal sulfide-based catalysts. These directions are for their practical use in water remediation.

Key words: Metal sulfides; Bimetallic sulfides; Advanced oxidation processes; Sulfur vacancies; Organic pollutant degradation

Citation: Bian F Q, Abbasi G H, Chen H, et al. Metal Sulfide-Based Catalysts for Advanced Oxidation Processes: Tailoring Strategies and Mechanistic Insights for Organic Pollutant Removal. *Environmental Chemistry and Safety*, 2025, 1, 9600046. https://doi.org/10.26599/ECS.2025.9600046

1. Introduction

Safe and clean water is of vital importance to public health and socio-economic development. However, the continuous urbanization, the rising population pressure and the rapid economic development pose a huge threat to the global water quality [1,2]. The traditional wastewater treatment system has several limitations. They are confronted with problems such as high operating costs, inconsistent and often poor pollutant removal efficiency, generation of secondary pollutants, difficulty in treating toxic sludge, and complex equipment setup. Because of these drawbacks, it is imperative that improved wastewater treatment techniques be developed. These techniques need to be efficient, stable and economically viable. The advanced oxidation processes (AOPs) have received extensive attention in wastewater treatment. Many organic contaminants can be entirely broken down by them or changed into less hazardous and more biodegradable compounds. And they are more appealing due to their potent oxidation efficacy and lack of secondary pollutants [3-5]. Although AOPs are effective, they have drawbacks of their own. These problems include low catalyst stability, large oxidant dosage and narrow operational pH range, all of which hinder their wide application. Take the Fenton system as an example. Due to poor electron transfer, the rate at which Fe^{3+} is transformed into Fe^{2+} is very slow. What's more, the process often needs lots of chemicals. These chemicals acidify the wastewater to pH 2–4 before treatment, and the water must be neutralized before being released. Iron sludge builds up too. This further hurts the Fenton system's efficiency and stability [6]. Titanium dioxide-based catalysts also have drawbacks. These are low electrical conductivity, a wide bandgap, fast electron–hole recombination, and low activity under visible light. All these greatly limit how well they work in AOPs [7].

Vanadates are another key group of photocatalytic materials in advanced oxidation catalysts. Examples include $BiVO_4$ and Ag_3VO_4. They have caught much research attention due to their narrow band gaps, strong visible-light response, low cost, and excellent crystallinity. However, they often encounter issues. Rapid electron-hole recombination and low charge carrier mobility are common [8]. Metal sulfides, by contrast, are some of the most abundant natural materials. They have got a lot of research interest in recent years.This is due to

Correspondence to: Chen H, chenhong@swu.edu.cn; Liu L D, lindongliu@swu.edu.cn

Received: September 16, 2025; Revised: November 17, 2025; Accepted: November 25, 2025

their affordability and accessibility. Adding electronegative sulfur helps electrons spread out across the catalyst structure. This creates efficient electron-transfer paths, which encourage metal cations to move toward S [9]. Metal sulfides Metal sulfides also have their unique properties. This includes a wide range of components and forms, chemical stability in oxidizing environments, low redox potential, electron-rich surfaces and superior electrical conductivity. These features make them ideal choices for wide application. Among these applications, there is the Advanced Oxidation process (AOPs) (Fig. 1).

Many studies have shown that monometallic transition metal sulfides can be well used as catalysts. For instance, MoS_2, WS_2, FeS_2, CoS_2 and ZnS all have excellent catalytic capabilities. However, studies on bimetallic sulfides have shown that they are more effective. They decompose organic pollutants more effectively than monometallic systems [10-12]. For this reason, adding extra metals has become a good method. These include redox-active metals (e.g., Fe, Co, Cu, Mn) and electron-rich metals (e.g., Mo, W, V) to produce bimetallic sulfides. This increases the service life and efficiency of the catalyst in wastewater treatment.

This review examines metal sulfides in detail. It covers their structure, properties, and how they work in AOPs. It also suggests ways to improve metal sulfide-based catalysts. These ways include using bimetallic sulfides, bimolecular non-metal sulfides, and other supporting methods. And the goal is to boost their performance, stability, and efficiency. These findings point to useful ways to create new solutions for solving water pollution.

2. Structural and Property Profiling of Metal Sulfides

2.1. Crystal Structures of Metal Sulfides

Metal sulfides have a variety of crystal structures. Their shapes are mostly determined by the metal and sulfur ions' ionic dimensions, charge states, and kind of bonding. And their chemical reactivity is largely influenced by these structural characteristics. Pyrite (FeS_2), for example, its iron ions and disulfide groups are arranged in a certain way in the lattice. This makes it very easy to break down when oxidized in air. In this section, we look at the crystal forms of some monometallic sulfides, seeking to explain the basic mechanisms by looking at their structures [13].

2.1.1. CuS

Copper sulfide (CuS) has caught a lot of research interest because it's cost-effective and has an easy-to-make synthesis process [14]. It usually forms a hexagonal crystal structure. This structure has tightly packed Cu–S and S–S layers alternate. And weak van der Waals forces hold these layers together. Cu–S bonds have relatively low energy, making the structure easy to break down when heated. Higher temperatures make atoms vibrate more. This causes bonds to split, leading to decomposition or oxidation afterward. CuS has a BET surface area up to 11.9 m^2/g, which is much higher than MnS (3.6 m^2/g), CoS (2.0 m^2/g) and FeS (0.8 m^2/g) [15]. Its surface has a

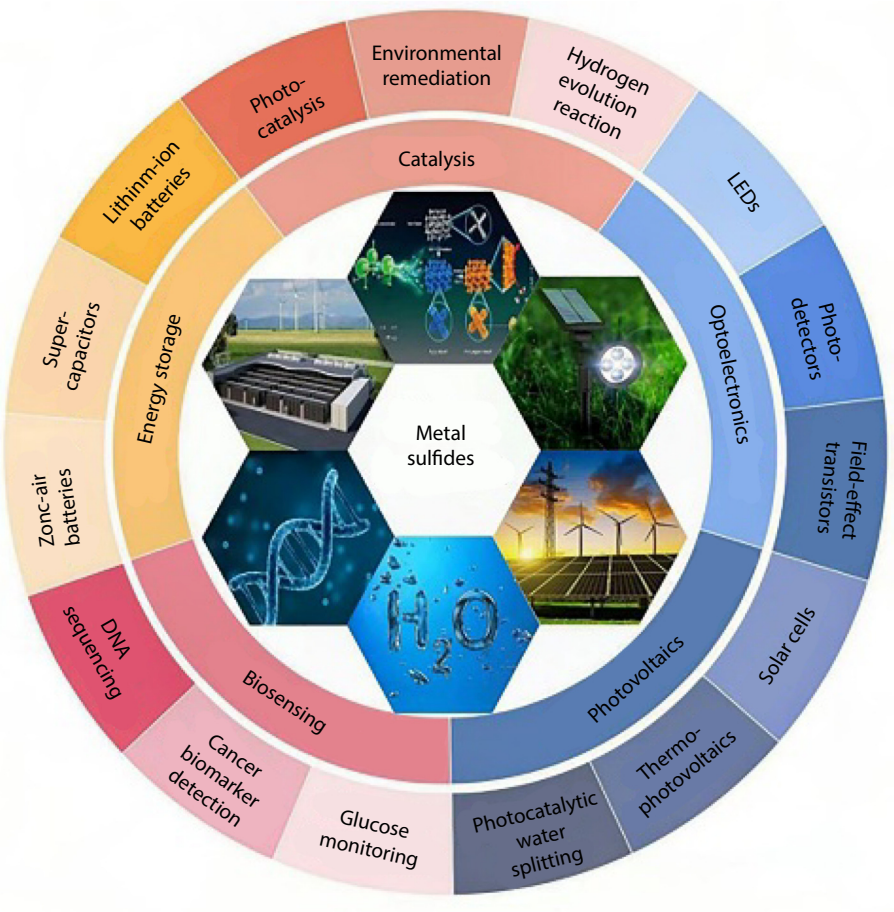

Fig. 1. The employability of metal sulfides in multifaceted disciplines. Reproduced with permission [5]. Copyright 2024, Coordination Chemistry Reviews.

fine, porous texture, providing lots of active sites. These sites catalyze the decomposition of H_2O_2very well, generating·OH radicals. The catalyst remains stable under reaction conditions. It can also maintain good performance over a wide pH range. In combination with other catalysts, such as Fe^{2+}, can further boost the efficiency of Fenton-like processes [16]. Another method is to construct heterojunctions with substrates such as graphene or TiO_2. This improves the separation of photogenerated charge carriers, thereby enhancing the catalytic performance [17].

2.1.2. ZnS

Zinc sulfide (ZnS) is receiving increasing attention in research. This increased attention is due to its remarkable thermal stability. As the main part of zinc concentrate ore, it mainly exists as sphalerite, wurtzite, and matraite. Sphalerite has a face-centered cubic structure. Zinc and sulfur ions here are arranged in a tetrahedral coordination, while wurtzite and its trigonal variant correspond to hexagonal and rhombohedral polytypes respectively [18](Fig. 2(a-b)). The S and Zn vacancies in the ZnS lattice serve as active sites. They adsorb H_2O_2 and organic molecules, helping to form free radicals in Fenton-like systems. ZnS is a type of II-VI semiconductor with a wide bandgap and is regarded as a promising photocatalyst for water purification. Reasons for this include efficient charge transport, high electron mobility, non-toxicity, water insolubility, and affordability [19-21]. When exposed to light, ZnS produces electron-hole pairs. These pairings facilitate the decomposition of H_2O_2 into ·OH, participating in Fenton-like reactions [22].

2.1.3. MoS_2

Molybdenum disulfide (MoS_2) is used more and more in persulfate-driven AOPs (PS-AOPs), because it has good traits like natural abundance, low cost, good biocompatibility, and easy exfoliation into mono- or few-layer 2D forms [23-25]. Each layer has a sandwich structure of S–Mo–S. Its thickness is about 0.62 nm, and the gap between adjacent layers is 0.30 nm [26]. Atoms inside each layer are held together by covalent bonds, while adjacent layers stack up through weak van der Waals forces. The in-plane lattice parameter is a = 3.09 Å, and the length of the Mo–S bond is 2.39 Å [27]. MoS_2 mainly comes in three polytypes. These are 1T (octahedral), 2H (hexagonal), and 3R (rhombohedral) [28] (Fig.2(c-d). The 1T phase has trigonal antiprismatic coordination. Here, each Mo atom is surrounded by six S atoms in an octahedral shape [29]. The 2H polytype is similar to graphite. It has an indirect bandgap of 1.29 eV and is the most stable form. The rhombohedral 3R phase is less studied. But it shows potential in photonic and electrochemical applications [30-31]. Both 2H and 3R phases of MoS_2 have trigonal prismatic coordination around Mo atoms. But they differ in stacking order and the number of "MoS_2" layers in their unit cells. The 2H-MoS_2 phase has two layers per unit cell. These stack in an AB-AB sequence. The 3R-MoS_2 phase has three layers, and they are arranged in an ABC-ABC sequence [28]. As Zang et al. noted, most research focuses on the metallic 1T and semiconducting 2H phases. The 3R phase remains underexplored owing to the lack of reliable methods for its controlled synthesis, high-purity production, and large-scale fabrication. Although environmental research has focused on 1T and 2H types, studies on the 3R structure remain limited [32]. In 2H-MoS_2, catalytic sites are mostly at the edges. They also exist at S vacancies in the basal planes. These vacancies change the electronic environment and increase the negative charge density on Mo atoms.

2.1.4. WS_2

Tungsten disulfide (WS_2) has a layered structure, composed of a tungsten layer sandwiched between two layers of sulfur. These layers are held together by weak van der Waals forces. This configuration gives WS_2 an extensive specific surface area. It also provides lots of exposed edge sites, serving as reactive centers. The vacancies of sulfur (S) and tungsten (W) in WS_2 act as catalytic sites by absorbing reactant substances and promoting the generation of radicals. He et al. reported findings regarding WS_2. As a cocatalyst, it promotes the Fe^{3+}/Fe^{2+} cycle through redox reactions. These reactions involve exposed W^{4+} sites and Fe^{3+}. ·OH and $O_2^{\bullet-}$ radicals are the main drivers of this process [33].

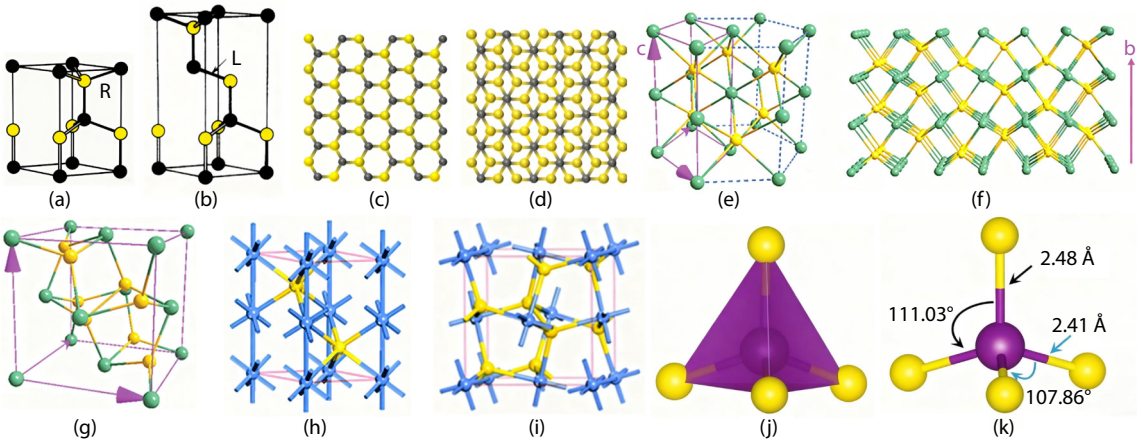

Fig. 2. The wurtzite crystal structure is (a), and the sphalerite crystal structure is (b). Reproduced with permission [19]. Copyright 2011, Progress in Materials Science. (c) Atomic positions in the 2H phase with trigonal prismatic coordination, and (d) atomic positions in the 1T phase with octahedral coordination. Reproduced with permission [26]. Copyright 2017, Environmental science & technology. (e) (f) Crystal structure of troilite (FeS) viewed along different orientations. Reproduced with permission [34]. Copyright 2014, Nanoscale. (g) Crystalline structures of pyrite FeS_2. Reproduced with permission [34]. Copyright 2014, Nanoscale. (h) illustrates the crystal structure of α-NiS, and (i) shows the crystal structure of NiS_2. Reproduced with permission [54]. Copyright 2024, Nanoscale Advances. (j) Optimized crystal structure model for α- involving MnS, and (k) for γ-MnS. Reproduced with permission [50]. Copyright 2024, Small.·OH is the main species that breaks down organic pollutants [53].

2.1.5. FeS

Up to now, eight polymorphs of ferrous sulfide (FeS) have been found. They form crystals in cubic, monoclinic, orthorhombic, tetragonal, and hexagonal systems. These structures are grouped into types like troilite, pyrrhotite-, mackinawite-type, and their variants. Most FeS polymorphs have a troilite-type structure within the hexagonal space group P62c. Each FeS_6 unit shares edges with nearby units along the a-axis or c-axis [34-35](Fig. 2(e-f)). In FeS/PMS systems, high-valent iron (Fe(IV)) is the main active substance [15]. FeS works in two ways. It acts as both an adsorbent and a catalytic activator, with Fe(II) and S(-II) working together to donate electrons—this is key for pollutant degradation [36]. Hong et al. shared their research on FeS. It effectively activates PMS to remove organic pollutants, where S(-II) boosts the Fe^{3+}/Fe^{2+} cycle. It does this by shuttling electrons through Fe–S coordination bonds, thus improving the regeneration of active iron sites [37].

2.1.6. FeS_2

Iron disulfide (FeS_2) has got a lot of attention from researchers. It's cheap, easy to find in nature, and has plenty of Fe^{2+} active sites—this is especially true for its use in environmental remediation [37]. It mainly comes in two crystal forms. One is pyrite, with a cubic lattice (space group Pa3). Each Fe atom here is surrounded by six S atoms in an octahedral arrangement [38]. The other is marcasite. It has an orthorhombic structure (space group Pnnm) [39] (Fig. 2(g)). In Fenton processes, Fe^{2+} reacts with H_2O_2. This reaction makes hydroxyl radicals, and these have a high oxidation potential (2.8 eV) [40]. They can break down almost all organic pollutants into CO_2 and H_2O [41]. Photo-Fenton catalysis further addressed the issue of limited cycling efficiency of Fe^{2+}/Fe^{3+} [42-43].

2.1.7. NiS

Nickel sulfide (NiS) is recognized for its high stability and cost-effectiveness. Its narrow band gap (1.92–2.41 eV) also makes it an effective photocatalytic material [44]. NiS has two main crystal structures. These are hexagonal system (α-type) and trigonal system (β-type), and temperature determines which one forms. Its catalytic active sites include surface Ni^{2+}/Ni^{3+} pairs and S vacancies. These sites adsorb reactants and help create radicals. The α-NiS phase has a hexagonal structure like niccolite. Ni atoms here are octahedrally coordinated, and there's clear metal–metal bonding (Ni–Ni distance ≈ 2.68 Å). Cubic NiS_2 is another common form. It has a pyrite-type structure with separate S_2 units [45] (Fig. 2(h-i)). The β-NiS phase has a rhombohedral unit cell. Sajjad Haider and his team studied NiS and NiS–carbon nanotube (CNT) nanocomposites. They found these materials have a large surface area. This large surface area boosts redox reactions and enhances electron transfer. Both effects help improve catalytic performance [46-47].

2.1.8. CoS

Cobalt sulfide (CoS) stands out for its active redox behavior [48-49]. It usually forms crystals in hexagonal or orthorhombic systems. Its surface has active sites. These include Co^{2+}/Co^{3+} couples and S vacancies, which help break down H_2O_2 or persulfates into highly reactive radicals. In CoS/PMS systems, the main reactive species are Co(IV) and $^1O_2$ [15]. CoS also has a very high specific surface area. This helps to adsorb organic pollutants, increase their local concentration and improve the degradation efficiency.

2.1.9. MnS

Manganese sulfide (MnS) has several crystal phases. The most stable one is α-MnS. It has a rock salt structure, with tetrahedral coordination. γ-MnS is different—it has a wurtzite-type structure. Its Mn–S bonds form an isosceles tetrahedral shape: three short bonds and one long one. This shows the bonding interactions are weaker [50] (Fig. 2(j-k)). β-MnS has a zinc blende structure, and this form is metastable. MnS's surface active sites include Mn^{2+}/Mn^{3+} redox pairs and sulfur vacancies, catalyzing the decomposition of H_2O_2 or persulfating to make reactive radicals [51]. Manganese can exist in three oxidation states: Mn(II), Mn(III), Mn(IV). The conversion between these states helps turn O_2 into $O_2^{\bullet-}$, and then into ·OH [52]. In oxidation processes [53].

This section provides a detailed introduction to metal sulfides. The relationship between their crystal structures and the catalytic performance of the Fenton-like reactions was mainly studied. The sulfides under discussion include CuS, ZnS, MoS_2, WS_2, FeS, FeS_2, NiS, CoS and MnS. We focus on the inherent structural features of these materials, which enhances our understanding of their fundamental characteristics. Our analysis pointed out the key structural features that drive catalytic activity: 1. Their electron band structure is adjustable. For example, NiS has the narrow bandgap. This endows the material with a remarkable ability to absorb light and separate charges. 2. Their surfaces have a large number of active sites. These include metal atoms with unsaturated coordination at the edges, such as Mo in Mo_2. They also include redox-active metal pairs, such as $Co^{2+}/Co^{3+}$and Ni^{2+}/Ni^{3+}. Sulfur and metallic vacancies are prevalent as well. These sites help activate hydrogen peroxide or persulfates (PMS/PDS) efficiently. 3. Some have layered shapes—MoS_2 and WS_2 are good examples. Others like CuS have a high specific surface area. Both provide lots of reactive interfaces. 4. They contain reducible components. FeS has S^{2-} and Fe^{2+}, for instance. These components promote smooth metal valence cycling—like the Fe^{3+}/Fe^{2+} cycle. This cycling keeps radical species (·OH, $SO_4^{\bullet-}$) or non-radical active oxygen species ($^1O_2$, Fe(IV), Co(IV)) being produced.

Although we've made good progress in research, there are still challenges to overcome. For one thing, we still haven't fully explored metal sulfides. Take certain crystal phases as examples. The 3R phase of MoS_2 and the many polymorphs of NiS—their potential in environmental catalysis is just starting to be studied. We also lack systematic comparative studies. These would look at their performance advantages and stability in detail.

2.2. Electronic Structures of Metal Sulfides

The electronic structure of transition metal sulfides (TMS) is formed by the mixture of the d orbitals of transition metals and the p orbitals of sulfur. This mixture generates covalent bonds within the material layers. Weak van der Waals forces press these layers against each other. Because sulfur has a very high electronegativity, it absorbs electron density from metal atoms. This makes the bonds have both ionic and covalent traits. Therefore, the chemical bonds of metal sulfides are neither pure ionic bonds nor pure covalent bonds. It lies somewhere in between. Metal cations can have multiple oxidation states in TMS. This ability helps electrons move through the

material—critical for activating oxidants and catalyzing redox-based pollutant breakdown [5]. These attributes make TMS highly suitable for use in AOPs.

Band theory utilizes bands to help explain the electronic properties of metal sulfides. The gap between the valence band and conduction band—we call this the band gap—represents the minimum energy needed to push an electron into a conductive state [55-56]. Some metal sulfides have energy bands like metals do. Their conduction bands and valence bands are easily accessible. When these sulfides are stimulated sufficiently, electrons can transition from the valence band to the conduction band. This lets electricity flow through them. Conversely, other metal sulfides act as semiconductors. They have a clear band gap between the two bands. External energy—like heat or light particles—can push electrons across this gap. This creates electron–hole pairs, which makes the material conductive.

In summary, metal sulfides have unique traits. These include good electrical conductivity, a relatively low redox potential, and an electron-rich nature. These traits are key to boosting their effectiveness in AOPs. This is especially true when they act as co-catalysts to regenerate active sites. For instance, its high electrical conductivity enables electrons to pass through the catalyst rapidly, which is a key factor driving redox reactions in the AOPs process. This property lets metal sulfides take an active part in electron-exchange processes. What' s more, metal sulfides have low redox potential and lots of electrons. Together, these two things let them donate electrons easily. This electronic empowerment helps to reduce metal ions and aids in regenerating active sites on the catalyst surface.

3. Advanced Oxidation Mechanisms in Transition Metal Sulfide-Based Systems

AOPs is a very promising approach to dealing with environmental issues. They can reduce the chemical oxygen demand (COD) and remove emerging pollutants. TMS have a large number of sulfur sites and redox sites. They also have built-in catalytic activity and adjustable electronic structures. So they're seen as effective catalysts in AOPs [15]. A key part of these processes is making reactive oxygen species (ROS) efficiently from catalysts, oxidants, and the reaction medium [57]. ROS forms in two main ways: radical and nonradical pathways. For the radical pathway, the catalyst activates the oxidant, such as H_2O_2, persulfates (PMS and PDS), and ozone (O_3). This will produce free radicals such as $SO_4^{\bullet-}$, ·OH, and $O_2^{\bullet-}$[58]. TMS facilitates accelerated oxidation by utilizing its distinctive electrical configuration, surface active sites, and metal-sulfur synergy. The core of this process is to generate highly oxidized radicals. This occurs through changes in the valence of transition metals, surface defects (e.g. sulfur vacancies), and the activation of oxidants, all of which can effectively decompose pollutants. Nonradical oxidation occurs on the surface of the catalyst. It mainly goes through three routes: electron transfer (ETP), $^1O_2$ oxidation, and high-valent metal-mediated oxidation [3,59,60].

3.1. Mechanism of Redox-Active Metal Sulfides

3.1.1. CuS

CuS is a naturally occurring sulfide mineral. It has metallic conductivity and a unique layered structure [61]. Sulfur species (S^2, Sn^2) donate electrons to rejuvenate metal sites. The catalytic activity of CuS stems from the redox copper pairs (Cu (I)/Cu(II)) and these sulfur compounds (such as S^{2-}, Sn^{2-}). These sulfur components play a crucial role in facilitating the movement of electrons, which is essential for the Cu(I)/Cu (II) redox cycle. This boosts PMS activation and pollutant degradation [62-64]. In the CuS/PS system, most reactions are heterogeneous. They take place on the catalyst's surface. PS sticks to CuS and gets activated to generate ROS, mainly SO_4•- and ·OH. Meanwhile, PS oxidized the ionic bonds in CuS. This forms Cu^{2+} and S^{2-}. Then S^{2-} gets oxidized into various intermediate-valence sulfur species. These aren't final products. They're better at reducing than S^{2-}. These species act as efficient catalytic shuttles. They quickly turn Cu(II) back into Cu(I), which is key for keeping the Cu(I)/Cu(II) cycle going. Although homogeneous activation is limited, dissolved Cu^{2+} can still activate PS in solution. This generates $SO_4^{\bullet-}$ and ·OH [65] (Table1). When copper catalysts activate PMS, the Cu(II)/Cu(I) cycle helps make ·OH, while the Cu(III)/Cu(II) cycle produces $SO_4^{\bullet-}$ [66] (Fig. 3(a)).

3.1.2. FeS

FeS has strong reducing capacity and a thiophilic nature. This makes it highly reactive with various compounds [67-68]. In the FeS/PAA system, Fe(II) and S^{2-} are the primary initial con-

Table 1. Metal sulfide systems and their corresponding mechanisms.

System	Major Reactive Oxygen Species	Mechanism
CuS/PS	$SO_4^{\bullet-}$, ·OH	S^{2-} is further oxidized to intermediate sulfur species, which promotes the Cu(I)/Cu(II) cycle. The Cu(II)/Cu(I) cycle facilitates the formation of ·OH, while the Cu(III)/Cu(II) cycle gives rise to $SO_4^{\bullet-}$ [65-66].
FeS/PAA	·OH	During activation, Fe(II) is oxidized to Fe(III), generating •OH. Sulfur substances enhance the regeneration of Fe(II), thereby accelerating PAA activation and radical production [69].
NiS/PMS	$^1O_2$, $SO_4^{\bullet-}$,·OH	Ni^{2+} activates PMS to generate $SO_4^{\bullet-}$. Surface sulfur vacancies expose more Ni^{2+} active sites, enhancing PMS activation, while surface sulfur facilitates the regeneration of Ni^{2+} [73-75].
MnS/H_2O_2	·OH	The efficient cycling between Mn(II)/Mn(III)/Mn(IV) provides sufficient $O_2^{\bullet-}$, thereby generating additional ·OH to enhance the degradation of organic pollutants [53].
MoS_2/PS	·OH	Mo(IV) is oxidized to Mo(V) and Mo(VI), with Mo(V) likely being the primary factor in the selective activation of PMS for $SO_4^{\bullet-}$ generation. Additionally, low-valent molybdenum reacts with O_2 to produce $O_2^{\bullet-}$, which is further converted to $^1O_2$ [91].
FeS_2/PS	SO_4•$^-$,·OH	FeS_2 releases Fe(III) through oxidation by PS, which activates PS to generate $SO_4^{\bullet-}$. $SO_4^{\bullet-}$ effectively degrades target organic pollutants. The oxidation process promotes the Fe^{2+}/Fe^{3+} cycle and enhances $SO_4^{\bullet-}$ production, while ·OH may be generated from $SO_4^{\bullet-}$ [88-89].

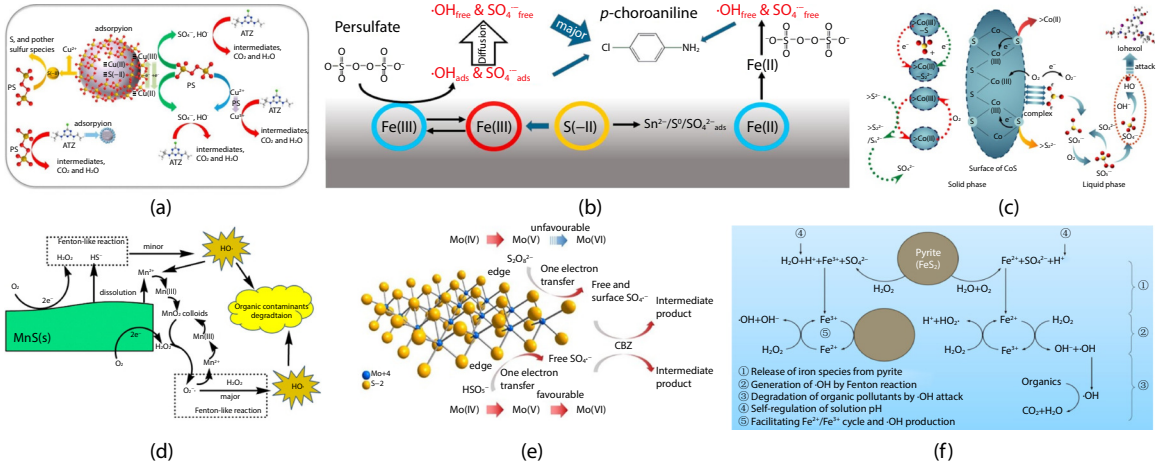

Fig. 3. (a) Probable mechanism in CuS/PS system. Reproduced with permission [65]. Copyright 2018, Chemical Engineering Journal. (b) Probable mechanism in FeS/PAA system. Reproduced with permission [69]. Copyright 2018, Chemical Engineering Journal. (c) The proposed mechanism of sulfite autoxidation by CoS. Reproduced with permission [76]. Copyright 2022, Chemical Engineering Journal. (d) Probable mechanism in MnS/H_2O_2 system. Reproduced with permission [53]. Copyright 2022, Science of The Total Environment. (e) Proposed activation mechanism of MoS_2 activated PMS and PS reaction. Reproduced with permission [91]. Copyright 2020, Chemical Engineering Journal. (f) Proposed mechanisms of pyrite-mediated Fenton oxidation processes for the degradation of organic pollutants. Reproduced with permission [87]. Copyright 2022, Water Research.

stituents. The surface Fe (II) oxidizes to Fe (III). This process generates ·OH and alkoxy radicals (R-O·). At the same time, the sulfur component oxidizes into elemental sulfur (S^0), S_8, and polysulfide ions (Sn^{2-}) [69-70] (Table1). These sulfur species help control how radicals form. Aqueous H_2S speeds up PAA activation and radical production by turning Fe(III) back into Fe(II). Sulfur species quickly use up R-O·, but ·OH is still the main radical that breaks down pollutants (Fig. 3(b)). The catalytic activity of FeS arises from the synergistic interaction between its variable-valent iron centers (Fe(II)/Fe(III)) and sulfur species. The sulfur components enable the essential conversion of Fe(III) to Fe(II), thus improving the activation of PAA and consequently advancing contaminant degradation.

3.1.3. NiS

Nickel-based catalysts work well to activate PMS. They break down many different organic pollutants [71]. Luo et al. designed NiS with sulfur vacancies. They found key active sites for PMS activation: Ni^{2+}, reduced sulfur species, and sulfur vacancies [72]. Sulfur vacancies expose more Ni^{2+} sites, which improves PMS activation, while surface sulfur helps regenerate Ni^{2+}. Activating PMS produces $SO_4^{\bullet-}$, which can react with H_2O or OH^- to form ·OH. Both radicals stay attached to the catalyst surface. $^1O_2$ forms in two ways: either from $O_2^{\bullet-}$ combining, or from $O_2^{\bullet-}$ reacting with H_2O or ·OH[73-74]. Additionally, PMS can be directly oxidized at sulfur vacancies to make $^1O_2$ [75] (Table1). And the catalyst acts as a mediator for electron transfer here [71].

3.1.4. CoS

Cobalt sulfide (CoS) has active sites on its surface. These include Co^{2+}/Co^{3+} redox pairs and sulfur vacancies, which effectively help break down H_2O_2 or persulfates. This breakdown creates highly reactive radical species, and these radicals go on to degrade pollutants. CoS has strong redox activity. This is because Co(II) can activate substances well, and sulfur species can give away electrons [76]. In the CoS/S(IV) system, organic pollutants are removed in two ways. One is homogeneous (using dissolved Co^{2+}), the other is heterogeneous (using Co on the surface) [77]. In the CoS_2/PMS system, several ROS help with catalysis. These are $^1O_2$, ·OH, and $SO_4^{\bullet-}$—and $SO_4^{\bullet-}$ plays the biggest role [78]. Initially, Co^{2+}sites on the surface react with PMS. This forms $SO_4^{\bullet-}$ and Co^{3+}. Then the radicals oxidize pollutants, and PMS turns Co^{3+} back into Co^{2+}, which completes the catalytic cycle [79] (Fig. 3(c)).

3.1.5. MnS

Liao et al. [53] showed that MnS dissolution in acidic conditions. This releases sulfides, which activate molecular oxygen on MnS surfaces. They use a two-electron transfer pathway to make H_2O_2 [80]. Sulfides also act like a Fenton-like reagent. They activate H_2O_2 to produce ·OH. This ·OH oxidizes Mn(II) to Mn(III), which further turns into Mn(IV) and reacts with H_2O_2 to form $O_2^{\bullet-}$. At the same time, Mn(II) and $O_2^{\bullet-}$ can also form Mn(III). $O_2^{\bullet-}$ and Mn(II)/Mn(III)/Mn(IV) cycle efficiently. This provides $O_2^{\bullet-}$ for Fenton reactions, making more ·OH to boost degradation [53] (Table1). Wang et al. put forward an idea about the Mn(II)/sulfite system. Sulfite oxidizes by itself to form $SO_3^{\bullet-}$. O_2 then oxidize $SO_3^{\bullet-}$s to $SO_5^{\bullet-}$, which drives Mn's redox cycling [81-84]. $SO_5^{\bullet-}$ and $SO_4^{\bullet-}$ oxidize Mn(II) to Mn(III) and Mn(IV), while Mn(III) speeds up sulfite consumption, creating more $SO_5^{\bullet-}$ and $SO_4^{\bullet-}$ [85] (Fig. 3(d)).

3.1.6. FeS_2

There are catalytic sites on the crystal surface of FeS_2. These include variable-valence iron centers (Fe(II)/Fe(III)) and reducing sulfur species, such as S^{2-} and S_2^{2-}. Surface Fe (II) and Fe (III) ions are the main active centers for activation by direct oxidants. They transfer electrons with H_2O_2 or persulfates (PMS/PDS) to start radical chain reactions.At the same time, reducing sulfur species work as key promoters and electron storage units. They work well to convert Fe(III) back to Fe(II). The suggested Fenton-like oxidation mechanism has several key steps. These are iron dissolving from the mineral surface, ·OH forming via Fenton reactions, and the resulting free radicals oxidizing and breaking down organic pollutants. O_2oxidizes FeS_2

and makes it dissolve, releasing Fe(II). This Fe(II) takes part in Fenton chemistry. In addition, H_2O_2 can oxidize FeS_2 to form Fe(III)[86]. FeS_2 and Fe^{3+} interact in two ways.They promote Fe^{3+} reduction to Fe^{2+} in solution. They also speed up Fe^{2+} release from the FeS_2 lattice. This means FeS_2 enhances the Fe^{2+}/Fe^{3+} cycling, which is needed for continuous ·OH production and efficient organic pollutant degradation [87].

When FeS_2 activates PS oxidation, there's another pathway besides $O_2^{\bullet-}$-mediated oxidative dissolution. FeS_2 may be directly oxidized by PS to release Fe(III). Both PMS and PDS can be activated to generate $SO_4^{\bullet-}$. Persulfates directly oxidizing FeS_2 also leads to $SO_4^{\bullet-}$ formation [88]. This radical attacks organic pollutants, resulting in efficient breakdown. During the whole process, Fe^{3+} reacts with FeS_2. This further helps reduce Fe^{3+} to Fe^{2+} and releases more Fe^{2+} from the solid phase. This keeps the iron redox cycle going, allowing steady $SO_4^{\bullet-}$ generation. Researchers also believe that ·OH may be indirectly formed from $SO_4^{\bullet-}$ in the FeS_2/PS system [89] (Table1). Both radicals help break down pollutants. Moreover, sulfur species play a key role in FeS_2-driven oxidation. The system has sulfur in various valence states. These include monosulfides (S^{2-}), dissulfides (S_2^{2-}), polysulfides (Sn^{2-}), elemental sulfur (S^0), and sulfates (SO_4^{2-}). Among them, sulfur types with lower valence states are particularly conducive to promoting the cycle of Fe^{2+}/Fe^{3+} [87,90] (Figure 3(f)).

3.2. Mechanism of Electron-Rich Metal Sulfides

3.2.1. MoS_2

MoS_2 has active sites. These are mainly edge sites of its layered structure and sulfur vacancies on the basal planes. They help activate oxidants to make reactive oxygen species (e.g., ·OH, $^1O_2$). This activation lets pollutants in water break down efficiently. Layered MoS_2 works in persulfate-based AOPs. It's good at geting oxidants like PMS and PDS working directly, using electron and energy transfer mechanisms[25,59]. Mo (IV) gives electrons to oxidants. This process turns Mo(IV) into Mo(V) and then Mo(VI). Mo(V) is especially good at one job: it selectively breaks the peroxo bond (–O–O–) in PMS to form $SO_4^{\bullet-}$ [91] (Table1). Additionally, Mo(IV) reacts with dissolved O_2. This produces $O_2^{\bullet-}$, which can turn into $^1O_2$ by reacting with ·OH or H_2O_2. Early studies often used 2H-MoS_2. But recent research shows the 1T phase has better traits —it's metallic, transfers charge well, and adsorbs PMS more strongly [92-93]. The 1T phase mainly activates PMS to make $SO_4^{\bullet-}$, ·OH, and $^1O_2$. Vacancy defects, on the other hand, activate PDS to form ·OH, $^1O_2$, and $O_2^{\bullet-}$ [25]. In the Fenton-like system, MoS_2 serves as a cocatalyst. It accelerated the reduction of Fe3+ to Fe2+, promoted the decomposition of H_2O_2, and increased the output of ·OH. This is mainly attributed to the exposed Mo (IV) sites [94]. The Fe–MoS_2 catalyst with a higher 1T has more accessible active sites. They also transfer electrons better, which speeds up reaction kinetics [95-96] (Fig. 3(e)).

3.2.2. WS_2

WS_2 is a new type of transition metal dichalcogenide. It can be processed to get W(IV) active sites, showing great potential for water treatment [97]. In the Fe^{3+}/H_2O_2 system, WS_2 acts as a cocatalyst. It promotes Fe^{3+} reduction and H_2O_2 activation, generating ·OH and $O_2^{\bullet-}$ [98-99]. Unsaturated S atoms on the surface bind with protons to form H_2S. This creates sulfur vacancies, which expose W^{4+} sites. W^{4+} reduces Fe^{3+} to Fe^{2+}. Then Fe^{2+} activates H_2O_2 to produce ·OH [33].

3.3. Environmental Impact

3.3.1. pH

The pH value of the solution is a key parameter for wastewater treatment by AOPs. It greatly affects the decomposition of oxidants, controls the surface charge of TMS-based catalysts, and alters the physical and chemical properties of the target substrate [100-102]. Overall, pH influences degradation efficiency through multiple factors. These factors often work together. Their interactions create complex connections. Such factors include the redox potential of radical and non-radical species [103], the chemical form of persulfate [104], how much organic contaminants are protonated [105], and the availability of active sites plus overall catalytic performance [106]. But many current studies don't separate variables that might cause confusion. This makes it hard to link observed effects specifically to pH, or to figure out how much each factor contributes on its own [107].

3.3.2. Temperature

Temperature plays a fundamental role in PS-based AOPs. It has a significant impact on how pollutants decompose over time. In systems where free radicals are the main driving factor, higher temperatures within a specific range (e.g., 40-60°C or 40-80°C[108]) help to break the peroxygen (O-O) bonds in persulfates. This will lead to more aggressive production, thereby enhancing the efficiency of pollutant removal. But temperatures that are too high can cause radicals to cancel each other out—this happens because there are too many radicals. They might also trigger reactions between radicals and persulfate, shifting degradation toward non-radical pathways [109]. Temperature also changes how well catalysts work, whether the mechanism is radical or non-radical [110-111]. So far, few studies have looked at temperature effects in non-radical systems in a systematic way [112]. Part of the reason is that heating activates PS thermally at the same time, creating radicals that make it hard to interpret the mechanism clearly [107].

3.3.3. Coexisting substances

SO_4^{2-}, NO_3^- and Cl^- all exist in the system we studied. These ions have almost no influence on the reaction process. CO_3^{2-} and PO_4^{3-} were different—they greatly slowed down tetracycline (TC) removal. This is probably because they bind with metal sites on the catalyst surface, blocking the active centers [15,113-114].

But coexisting ions don't always have the same impact. It depends on the specific reaction system. Take the CuS/PS system for atrazine (ATZ) degradation as an example. Researchers tested how Cl^-, HCO_3^-, and HPO_4^{2-} affect this process [65]. Cl^- slightly accelerated the degradation rate of ATZ. Because Cl^- reacts with $SO_4^{\bullet-}$ to form active chlorine species (RCS), such as Cl·, $Cl_2^{\bullet-}$ and Cl_2. These RCS have a very strong redox capacity. They break down ATZ in a way similar to $SO_4^{\bullet-}$ [115]. What's more, RCS help radical chain reactions keep going. This will produce more $SO_4^{\bullet-}$, thereby enhancing the degradation efficiency [116]. The addition of HCO_3^- also slightly promoted the degradation of ATZ. This anion reacts with $SO_4^{\bullet-}$ to form a bicarbonate radical (HCO_3·). These free radicals act as accelerators - they help PS decompose into $SO_4^{\bullet-}$, accelerating the degradation of ATZ. But if HCO_3^- concentration goes over a certain level, ATZ removal drops sharply. That's because HCO_3^- starts

competing with ATZ for both ·OH and $SO_4^{\bullet-}$ [117]. In the end, this has a net negative effect on degradation. HPO_4^{2-}, on the other hand, always slowed down ATZ degradation. There are two main reasons for this: 1. HPO_4^{2-} reacts with $SO_4^{\bullet-}$ and ·OH to form $HPO_4^{\bullet-}$. These radicals aren't strong enough to oxidize organic pollutants [118]. 2. HPO_4^{2-} sticks tightly to solid surfaces. It adsorbs onto the catalyst, reducing the number of available active sites [119].

3.3.4. Natural Organic Matter

Natural Organic Matter (NOM) is a complex mix. It's made of different organic compounds, with varying molecular sizes and properties. AOPs generate the powerful oxidant ·OH. This ·OH can react with NOM [120]. So NOM acts as a ·OH scavenger—it uses up the radical. This lowers the degradation efficiency of target pollutants. Feng et al. ran a study to show this. They used humic acid (HA, 0–40 mg·L^{-1}) to stand for NOM, testing how it affects ketoprofen (KET) degradation. Results showed HA slowed down KET degradation. The more HA there was, the stronger the inhibitory effect. Several mechanisms explain this: 1. NOM can soak up radicals. It may even turn radical intermediates back into the original compounds. This messes with radical-based oxidation [103]; 2. HA has functional groups like carboxyl and hydroxyl. These groups easily react with $SO_4^{\bullet-}$ and ·OH [121-122]; 3. HA reacts strongly with these oxidants. It uses them up, which reduces the system's overall oxidative capacity [123].

Water matrix complexity also affects how well the system works. Feng et al. [123] pointed out something. KET degradation was least efficient in a seawater matrix as well. This is probably because seawater has high Cl^- levels. Cl^- soaks up $SO_4^{\bullet-}$ and ·OH, which cuts down KET degradation efficiency.

4. Regulation Strategies for Catalytic Performance Enhancement in Transition Metal Sulfides

4.1. Bimetallic sulfides

In recent years, transition metal sulfides have gotten a lot of attention. They're affordable, easy to design and make, and have strong catalytic activity [124-127]. Sulfur (S) is electronegative. Adding it to the catalyst makes electrons spread out more. This creates efficient paths for electron transfer and helps cations move toward sulfur. Lots of studies show single-metal transition metal sulfides work well as catalysts. But their performance often hits limits. Issues include too few active sites [128-129], slow metal valence cycling, and sometimes metal ion leaching or poor structural stability. To solve these problems, researchers produced bimetallic sulfides. Their main idea is to use the way two different metal elements work together. In contrast, bimetallic sulfides are better in several ways. They transfer electrons faster, have stronger electrochemical activity, and have more active centers. These characteristics stem from numerous redox reactions, band distortion and the formation of vertical heterostructures - all of which narrow the band gap [130]. So designing bimetallic sulfides or sulfide-based hybrid structures is a promising direction. This design uses the electronic interaction between two metals to boost catalytic function [9].

4.1.1. Co and M (M = Mn, Ni, Cu, Zn)

Conventional surface doping often causes catalyst leaching and poor stability [131]. Homogeneous bimetallic sulfides are different—their formation lets us adjust electronic structures precisely. They also create ideal metal–metal synergy, which greatly boosts catalytic performance [132]. Porous or hollow structures are really useful here. They have large surface areas and low density, which help expose more active sites [133-134]. So combining homogeneous bimetallic sulfides with hollow structures has become more and more popular. Metal-organic frameworks (MOFs) are a key type of crystalline porous material. They have various chemical compositions and work well in many applications [135]. MOFs is composed of metal nodes connected by organic molecules.These form a crystalline porous coordination network [136-138], maintain their structural stability through intermolecular forces, such as hydrogen bonds and π–π stacking [139-140]. They have a large surface area and adjustable chemical properties, making MOFs excellent precursor materials [141]. The organic skeleton can accommodate different metal ions. This enables the bimetallic system to be uniformly mixed at the molecular level [142].

For example, researchers made bimetallic MOF precursors by self-assembling $Co(NO_3)_2$, $M(NO_3)_2$ (where M = Mn, Ni, Cu, Zn), and 2-methylimidazole. M(II) and Co(II) have similar ionic radii and electronic structures. So M(II) ions take the place of Co(II) sites in the framework, instead of just staying on the surface. Then they used thioacetamide for sulfidation under hydrothermal conditions. This made hollow bimetallic sulfide polyhedra. Calcining them in a N_2 atmosphere further improved their crystallinity [143] (Fig. 4(a)) (Table2). In another

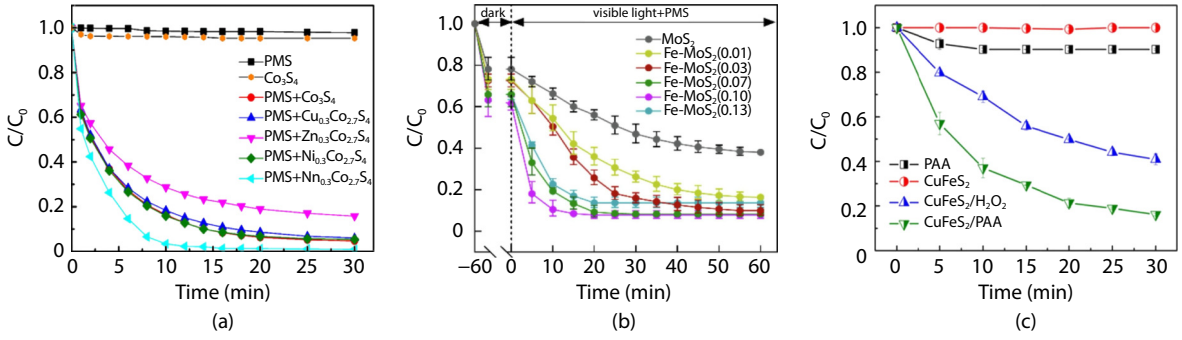

Fig. 4. (a) Degradation of SMT in the presence of different metal substituents. Reaction conditions: [SMT] = 55 mg L^{-1}, [PMS] = 0.3 g L^{-1}, catalyst = 80 mg L^{-1} and pH = 6.5. Reproduced with permission [143]. Copyright 2020, Chemical Engineering Journal. (b)Kinetics of TCH removal by Fe-MoS_2 composites with different molar ratios under light/PMS systems. Reproduced with permission [151]. Copyright 2022, Chemical Engineering Journal. (c) MTZ removal in diverse processe. Reaction conditions: [PAA] = 460 μM, [$CuFeS_2$] = 4 g L^{-1}, [H_2O_2] = 1278 μM, [MTZ] = 10 mg L^{-1}, [pH] = 3. Reproduced with permission [154]. Copyright 2023, Separation and Purification Technology.

Table 2. Enhanced pollutant degradation by modified metal sulfide catalysts

Pollutant	Oxidizing agent	Catalysts	Degradation rate (%)	Improved catalysts	Time (min)	Degradation rate (%)
SMT	PMS	Co_3S_4	<5	$Mn_{0.3}Co_{2.7}S_4$	15	100 [143]
				$Zn_{0.3}Co_{2.7}S_4$	30	85
				$Ni_{0.3}Co_{2.7}S_4$	25	95
				$Cu_{0.3}Co_{2.7}S_4$	25	95
BPA	PMS			$Mn_{0.3}Co_{2.7}S_4$	4	100
RhB	PMS			$Mn_{0.3}Co_{2.7}S_4$	10	100
TCH	PMS	MoS_2	39	Fe-MoS_2	15	100 [151]
PCA	PS	MoS_2	25.1	MoS_2-D/Fe^{3+}	30	100
MTZ	H_2O_2			$CuFeS_2$	30	59.07 [154]
	PAA					83.92

study, Li et al. made a core–shell structured cobalt–nickel sulfide ($NiCo_2S_4$/Co_9S_8/NiS, called NCS) using a two-step hydrothermal method. When used as a peroxymonosulfate (PMS) activator at pH 3.9, it removed 82.2% of pollutants in 35 minutes. This was much better than monometallic sulfides. The linked redox cycles of Co^{3+}/Co^{2+} and Ni^{3+}/Ni^{2+} were the key to this improved PMS activation [144].

4.1.2. Fe and Mo

Bimetallic Mo/Fe sulfides have plenty of active sites. They also show great potential for catalytic activation. These systems can be made using bimetallic MOF precursors [145-146]. Take Mo/Fe–MOFs as an example. They form 3D structures with alternating MoO_4^{2-}–Fe layers and 4,4′-bipyridine linkers [147]. Composites with closely interacting components expose more active sites. This makes their functionality stronger [146,148].

Previous studies point out something. Adding Fe into the MoS_2 lattice activates the basal planes—these are usually inactive. It also increases edge site exposure [149-150]. This greatly improves PMS activation. Li et al. made Fe-doped MoS_2 using a one-pot hydrothermal method. Its better performance comes from two things: (1) Structural changes let electrons move faster. (2) Fe–S–Mo bridges help electrons transfer efficiently. This allows Mo(IV)/Mo(VI) and Fe(III)/Fe(II) to cycle redox reactions to keep PMS decomposing [151] (Fig. 4(b)) (Table2).

4.1.3. Mo and M (M=Co, Ni)

Xie et al. made a heterostructured cobalt–molybdenum sulfide. It's supported on graphene oxide (O-CoMoS/GO) and has hierarchical nanosheets. This catalyst activates PMS really well. It removed nearly all 4-chlorophenol in just 10 minutes. Mechanism research showed the main reactive species are $^1O_2$, $SO_4^{\bullet-}$, and ·OH. Its high activity comes from the synergy between bimetallic sulfides and the GO support. GO enriches electron density on metal centers, moves the Co d-band closer to the Fermi level, and helps electrons transfer through Co/Mo–O–C interfaces [152].

Wang et al. did similar work. They made a nickel–molybdenum sulfide hybrid (L-$NiMoS_2$) with lots of active sites. This material has haloperoxidase-like activity. When H_2O_2 is present, it catalyzes the oxidation of Br^- to HOBr/OBr^-. Its catalytic rate constant was 135.7 times higher than that of pure MoS_2 [153].

4.1.4. Cu and Fe

Yang et al. utilized natural chalcopyrite ($CuFeS_2$) to activate peracetic acid (PAA) for metronidazole (MTZ) removal. The study confirmed that ·OH served as the primary degradative species, with surface Cu(I) and Fe(II) identified as key active sites. Sulfur atoms facilitated proton trapping, leading to sulfur vacancy formation and increased exposure of active sites, thereby promoting regeneration through reduced sulfur species [154] (Fig. 4(c)) (Table2).

4.2. Doped Non - metallic Elements

Doping with non-metallic elements provides an effective strategy for tuning the electronic and surface properties of metal sulfides [155]. Although cations typically serve as active sites in transition metal sulfides, adjacent anions significantly influence their electronic states [156]. Non-metal dopants can alter electronic structures via substitution or interstitial doping, modulating interactions between active centers and reactants/intermediates, and thereby regulating catalytic activity [157]. The large electronegativity difference between non-metals and metals facilitates electron transfer and orbital hybridization [158-159], reducing the band gap and promoting electron mobility. Additionally, lone-pair electrons on non-metal atoms can facilitate intermediate formation, enabling oxidation through non-radical pathways [160]. Incorporating non-metal elements into sulfide lattices has thus opened new avenues for designing tunable catalysts [155].

Recent research has shown that incorporating non-metal dopants into metal sulfides significantly improves their functional properties in diverse fields such as electrocatalysis (e.g., HER, OER, ORR), lithium/sodium/potassium-ion batteries, and photocatalysis. As an example, Wang and colleagues developed a heterojunction photocatalyst through a hydrothermal route, combining bismuth sulfide (Bi_2S_3) with non-metal doped graphitic carbon nitride (g-C_3N_4), designated as xCN-BS (x = O, S, or P). Using OCN-BS for the treatment of a 15 mg·L^{-1} bisphenol A (BPA) solution, a 96% removal rate was attained within 4 hours. The introduction of non-metal elements contributed to bandgap narrowing and electronic band structure optimization, which collectively enhanced both photocatalytic degradation efficiency and structural stability [161].

In another investigation, Ye et al. prepared nitrogen-doped iron disulfide nanoparticles (N-FeS_2) for application as an electrocatalyst in the HER. Nitrogen, with its high electronegativity, effectively modified the electronic states and band configuration of FeS_2. The resulting Fe–N interactions diminished electron density around sulfur atoms and weakened Fe–S bonds. Relative to pristine FeS_2, nitrogen doping elevated the surface electron density of N-FeS_2, which promoted the desorption of adsorbed hydrogen species (H*) and consequently enhanced H_2 production [162]. Similarly, Kou et al. reported

that nitrogen-doped nickel sulfide (N-Ni_3S_2) exhibited enhanced hydrogen adsorption capability [158].

In essence, non-metal doping presents several benefits such as cost-effectiveness, elevated stability, uniform dopant distribution, and reduced particle aggregation. Its impact on catalytic systems can be classified into four principal aspects: 1. Doping with non-metals customizes the electronic configuration of catalysts through modifications in electronic states, band alignment, and adsorption behavior [163-164]; 2. It augments catalytic kinetics by elevating the number of active sites and strengthening the intrinsic activity of catalytic centers [165-166]; 3. Enhanced charge transport capability accelerates electron transfer in electrocatalytic reactions, amplifying the intrinsic catalytic performance [167-168]; 4. Cooperative effects between dopant species and the host catalyst fine-tune the electronic environment of active sites and raise their density, resulting in a marked increase in electrocatalytic activity [169-170].

4.3. Introduction of Sulfur Vacancies

Introducing sulfur vacancies is a key defect engineering method for improving catalytic performance. Intentionally making sulfur-deficient sites changes physicochemical properties. It increases deformation energy, exposes active sites, and alters atomic coordination. The spread of electrons around these vacancies makes nearby metal atoms more reactive. This helps adsorbates break down and activates PMS —affecting both radical and non-radical pathways in AOPs [5,171]. For example, Kuang et al. created sulfur defects in MoS_2 through thermal annealing. This greatly enhanced Fe^{3+}/PMS activation. The catalyst with plenty of defects removed pollutants much better. This is because its surface charge was optimized and it adsorbed more Fe^{3+} [172] (Fig.5).

Stabilizing sulfur vacancies is really important. Main strategies are as follows: 1. Elemental Doping. Jiang et al. did defect engineering on MoS_2 by adding sulfur vacancies first. Then they doped In into the inner lattice of Vs-MoS_2. This method stabilized the catalyst well. It lowered the catalyst's surface energy and made sulfur redox reactions faster [173]. 2. Heterostructure Construction. Zhao et al. attached Vs-MoS_2 nanosheets to conductive defective graphene. This stabilized sulfur vacancies at a strong two-dimensional (2D-2D) interface. This setup made electrical contact between MoS_2 and the conductive substrate excellent. It also helped reactants reach active sites easily [174].

4.4. In Situ Regeneration of Catalytic Activity

Many metal sulfides work well for repeated use, but slow mass loss and active site consumption often hold back their long-term application [5]. For instance, MoS_2 loses its active sites quickly [25]. Useful ways to regenerate them include high-temperature pyrolysis in inert atmospheres —this turns oxidized Mo(VI) back to Mo(IV) [175]. UV light, and H_2O_2 treatment, which peels off layers to uncover new active sites, also work [176-178]. Other methods include adding elements, combining with co-catalysts, or making heterojunctions to direct charge transfer [179]. For example, Qu et al. made an FeOCl/MoS_2 membrane for non-stop PMS activation [180]. Carbon supports have real advantages too; their large surface area lets us build 3D MoS_2@carbon structures. Zhu et al. designed a 3D MoS_2 sponge. It kept 97.87% degradation efficiency for antibiotic wastewater during 16 days of non-stop use [181].

5. Conclusion and outlook

Based on single-metal sulfides, bimetallic sulfides have great potential in AOPs. They are particularly effective in environmental restoration and wastewater treatment. They have a synergistic effect and a unique electronic structure, so they fully utilize the interaction between the two metals. This enables them to effectively activate oxidants such as persulfate and hydrogen peroxide. The activation produces highly reactive free radicals (e.g., $SO_4^{\cdot-}$ and ·OH), which break down organic pollutants effectively. Bimetallic sulfides are also tunable and diverse. These characteristics endow it with good catalytic activity, stability and recyclability. We also suggest using non-metallic sulfides in a smart way. This helps adjust catalytic activity effectively. Adding sulfur vacancies and in-situ regeneration methods too can greatly expand what metal sulfides can do in AOPs. But current research still faces some challenges. These issues include the complexity of material synthesis methods, incomplete understanding of reaction mechanisms, and problems with large-scale application in actual wastewater treatment. In conclusion, the research on bimetallic sulfides in deep oxidation holds broad prospects. Cooperation in different fields and the proposal of new technological concepts can enable these materials to provide new methods for controlling environmental pollution and supporting sustainable development.

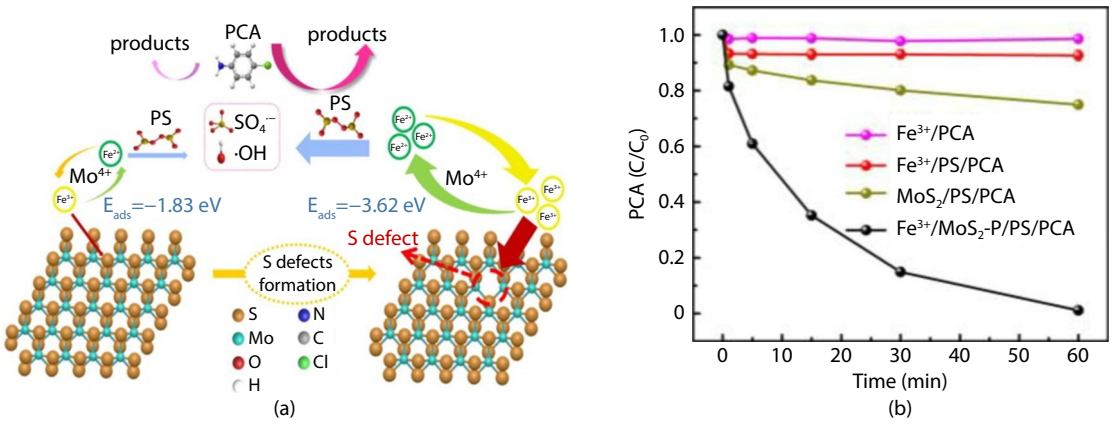

Fig. 5. (a) Proposed mechanism, (b) Degradation of PCA by different PS activation systems. Reproduced with permission [172]. Copyright 2021, Chemical Engineering Journal.

To address these challenges and promote the transformation of basic research into practical applications, we suggest that future research focus be placed on the following promising directions:

1. Extensive Application of Non-metallic Doping in Advanced Oxidation Processes: Non-metallic doping is widely used in photocatalysis and electrocatalysis. But its potential in advanced oxidation still needs further study. This method changes the electron density of metal centers (e.g., Fe, Co, Cu). It makes it easier to activate oxidants (e.g., PMS, PDS, H_2O_2) to produce more reactive oxygen species. What's more, doping often creates defects and unsaturated sites. These naturally act as effective adsorption or catalytic centers.

2. Synergistic Multi-Strategy Design: Research should move away from just mixing single modification methods. Instead, it needs to truly figure out how different components work together. This better understanding helps build "superior catalytic architectures". These structures have strong inherent activity and stability.

3. Guidance for Density Functional Theory (DFT) calculations: DFT calculations provide a comprehensive image of the electronic and structural properties of metal sulfides at the atomic level. This theory is conducive to the ingenious design of new materials. These materials will have better catalytic activity, stability and electrical conductivity.

4. A Paradigm Shift towards Data-Driven Discovery: It is important to stop relying on guesses and repetitive testing. On the contrary, we should adopt a method based on understanding how things work. This means building large, fast-access databases. These databases link "synthesis-structure-property" relationships. We also need to combine machine learning (ML) and artificial intelligence (AI). These tools can improve metal sulfides' structural and composition traits, predict catalytic performance, and ultimately speed up the discovery of next-generation metal sulfide catalysts.

Acknowledgments

This research was funded by the Sichuan Science and Technology Program (grant 2023NSFSC0801), the Chongqing Municipal Education Commission (grants KJZD-K202500201, KJQN202200202 and KJQN202100214), and the Natural Science Foundation of Chongqing (grant CSTB2022NSCQ-MSX0448).

Conflicts of Interest

The authors declare that there are no conflicts of interest in this work.

References

[1] Zhu, Y. P.; Zhu, R. L.; Xi, Y. F.; Zhu, J. X.; Zhu, G. Q.; He, H. P. Strategies for enhancing the heterogeneous Fenton catalytic reactivity: A review. *Appl. Catal. B Environ.*, 2019, 255: 117739.

[2] Lu, F.; Astruc, D. Nanocatalysts and other nanomaterials for water remediation from organic pollutants. *Coord. Chem. Rev.*, 2020, 408: 213180.

[3] Duan, X. G.; Sun, H. Q.; Shao, Z. P.; Wang, S. B. Nonradical reactions in environmental remediation processes: Uncertainty and challenges. *Appl. Catal. B Environ.*, 2018, 224: 973–982.

[4] Miklos, D. B.; Remy, C.; Jekel, M.; Linden, K. G.; Drewes, J. E.; Hübner, U. Evaluation of advanced oxidation processes for water and wastewater treatment–A critical review. *Water Res.*, 2018, 139: 118–131.

[5] Ali, J.; Guo, S.; Chen, Y. N.; Shahzad, A.; Wajid Ullah, M.; Chen, F. X. Metal sulfides as emerging materials for advanced oxidation of wastewater: Recent developments, challenges, and prospects. *Coord. Chem. Rev.*, 2024, 509: 215765.

[6] Oturan, M. A.; Aaron, J. J. Advanced oxidation processes in water/wastewater treatment: Principles and applications. *a review. Crit. Rev. Environ. Sci. Technol.*, 2014, 44: 2577–2641.

[7] Tanos, F.; Razzouk, A.; Lesage, G.; Cretin, M.; Bechelany, M. A comprehensive review on modification of titanium dioxide-based catalysts in advanced oxidation processes for water treatment. *ChemSusChem*, 2024, 17: e202301139.

[8] El ouardi, M.; Arab, M.; Saadi, M.; BaQais, A.; Ait Ahsaine, H. Vanadate-based photocatalytic materials: A perspective on synthesis approaches and pollutants photocatalytic degradation. *Nano Mater. Sci.*, 2024

[9] Cai, J. J.; Liu, H. J.; Luo, Y. L.; Xiong, Y. Q.; Zhang, L. Z.; Wang, S.; Xiao, K.; Liu, Z. Q. Single-phase bimetal sulfide or metal sulfide heterojunction: Which one is better for reversible oxygen electrocatalyst. *J. Energy Chem.*, 2022, 74: 420–428.

[10] Chen, C.; Liu, L.; Guo, J.; Zhou, L. X.; Lan, Y. Q. Sulfur-doped copper-cobalt bimetallic oxides with abundant Cu(I): A novel peroxymonosulfate activator for chloramphenicol degradation. *Chem. Eng. J.*, 2019, 361: 1304–1316.

[11] Gao, J.; Liu, Y. T.; Xia, X. N.; Wang, L. L.; Dong, W. Y. $Fe_{1-x}Zn_xS$ ternary solid solution as an efficient Fenton-like catalyst for ultrafast degradation of phenol. *J. Hazard. Mater.*, 2018, 353: 393–400.

[12] Song, Y. B.; Sun, D. D.; Jiang, X. Y.; Ma, H. R.; Ma, C.; Hao, J.; Zhang, X. X. Enhanced activation of peroxymonosulfate by bimetallic spinel sulfides $CoNi_2S_4$ for organic dye degradation. *J. Environ. Chem. Eng.*, 2021, 9: 106889.

[13] Harrison, M. R.; Francesconi, M. G. Mixed-metal one-dimensional sulfides—a class of materials with differences and similarities to oxides. *Coord. Chem. Rev.*, 2011, 255: 451–458.

[14] Liu, D. J.; Li, C. E.; Jia, T.; Wu, J.; Li, B. Novel metal sulfide sorbents for elemental mercury capture in flue gas: A review. *Fuel*, 2024, 357: 129829.

[15] Zhao, Z. F.; Lin, L.; Liu, S. S.; Chen, Y. Q.; Daniels, S. V.; Xu, Z. J.; Chen, Z. H.; Li, H. T.; Wu, Y. Q.; Guo, L. L. et al. Unveiling the versatile performance of transition metal sulfides in peroxymonosulfate activation. *Chem. Eng. J.*, 2024, 497: 154682.

[16] Feng, C.; Zhang, H.; Ren, Y.; Luo, M. F.; Yu, S. Y.; Xiong, Z. K.; Liu, Y.; Zhou, P.; Lai, B. Enhancing zerovalent iron-based Fenton-like chemistry by copper sulfide: Insight into the active sites for sustainable Fe(II) supply. *J. Hazard. Mater.*, 2023, 452: 131355.

[17] Zheng, L. X.; Teng, F.; Ye, X. Y.; Zheng, H. J.; Fang, X. S. Photo/electrochemical applications of metal sulfide/TiO_2 heterostructures. *Adv. Energy Mater.*, 2020, 10: 1902355.

[18] Cook, N. J.; Ciobanu, C. L.; Pring, A.; Skinner, W.; Shimizu, M.; Danyushevsky, L.; Saini-Eidukat, B.; Melcher, F. Trace and minor elements in sphalerite: A LA-ICPMS study. *Geochim. Cosmochim. Acta*, 2009, 73: 4761–4791.

[19] Fang, X. S.; Zhai, T. Y.; Gautam, U. K.; Li, L.; Wu, L. M.; Bando, Y.; Golberg, D. ZnS nanostructures: From synthesis to applications. *Prog. Mater. Sci.*, 2011, 56: 175–287.

[20] Zhang, H. L.; Wei, B.; Zhu, L.; Yu, J. H.; Sun, W. J.; Xu, L. L. Cation exchange synthesis of ZnS–Ag_2S microspheric composites with enhanced photocatalytic activity. *Appl. Surf. Sci.*, 2013, 270: 133–138.

[21] Wang, W. M.; Lee, G. J.; Wang, P.; Qiao, Z. H.; Liu, N.; Wu, J. J. Microwave synthesis of metal-doped ZnS photocatalysts and applications on degrading 4-chlorophenol using heterogeneous photocatalytic ozonation process. *Sep. Purif. Technol.*, 2020,

237: 116469.

[22] Guo, Z. Y.; Huo, W. C.; Cao, T.; Liu, X. Y.; Ren, S.; Yang, J.; Ding, H.; Chen, K.; Dong, F.; Zhang, Y. X. Heterojunction interface of zinc oxide and zinc sulfide promoting reactive molecules activation and carrier separation toward efficient photocatalysis. *J. Colloid Interface Sci.*, 2021, 588: 826–837.

[23] Zhang, G.; Liu, H. J.; Qu, J. H.; Li, J. H. Two-dimensional layered MoS_2: Rational design, properties and electrochemical applications. *Energy Environ. Sci.*, 2016, 9: 1190–1209.

[24] Xu, Z. X.; Lu, J. C.; Zheng, X. Y.; Chen, B.; Luo, Y. M.; Tahir, M. N.; Huang, B.; Xia, X. S.; Pan, X. J. A critical review on the applications and potential risks of emerging MoS_2 nanomaterials. *J. Hazard. Mater.*, 2020, 399: 123057.

[25] Zhou, H. Y.; Xie, Z. H.; Liu, Y. M.; Lai, B.; Ong, W. J.; Wang, S. B.; Duan, X. G. Recent advances in molybdenum disulfide-based advanced oxidation processes. *Environ. Funct. Mater.*, 2022, 1: 1–9.

[26] Wang, Z. Y.; Mi, B. X. Environmental applications of 2D molybdenum disulfide (MoS_2) nanosheets. *Environ. Sci. Technol.*, 2017, 51(15): 8229–8244.

[27] Wang, J.; Zhang, W. T.; Yue, X. Y.; Yang, Q. F.; Liu, F. B.; Wang, Y. R.; Zhang, D. H.; Li, Z. H.; Wang, J. L. One-pot synthesis of multifunctional magnetic ferrite–MoS_2–carbon dot nanohybrid adsorbent for efficient Pb(ii) removal. *J. Mater. Chem. A*, 2016, 4: 3893–3900.

[28] Strachan, J.; Masters, A. F.; Maschmeyer, T. 3R-MoS_2 in review: History, status, and outlook. *ACS Appl. Energy Mater.*, 2021, *4*(8), 7405–7418.

[29] Wypych, F.; Solenthaler, C.; Prins, R.; Weber, T. Electron diffraction study of intercalation compounds derived from 1T-MoS_2. *J. Solid State Chem.*, 1999, 144: 430–436.

[30] Willatzen, M.; Wang, Z. L. Prediction of strong piezoelectricity in 3R-MoS_2 multilayer structures. *Nano Energy*, 2019, 56: 512–515.

[31] Li, S. S.; Lin, Y. C.; Zhao, W.; Wu, J.; Wang, Z.; Hu, Z. H.; Shen, Y. D.; Tang, D. M.; Wang, J. Y.; Zhang, Q. et al. Vapour-liquid-solid growth of monolayer MoS_2 nanoribbons. *Nat. Mater.*, 2018, 17: 535–542.

[32] Zang, L. L.; Wang, M. X.; Han, Q.; Wang, Z. Y. Phase-dependent properties and applications of MoS_2 in environmental remediation: Synthesis, characterization, and performance optimization. *ACS EST Water*, 2024, 4(11): 4690–4707.

[33] He, D. Q.; Wang, D. L.; Luo, H. W.; Zeng, Y. F.; Zeng, G. N.; Li, J.; Pan, X. L. Tungsten disulfide (WS_2) is a highly active co-catalyst in Fe(III)/H_2O_2 Fenton-like reactions for efficient acetaminophen degradation. *Sci. Total Environ.*, 2023, 871: 162151.

[34] Rui, X. H.; Tan, H. T.; Yan, Q. Y. Nanostructured metal sulfides for energy storage. *Nanoscale*, 2014, 6: 9889–9924.

[35] Xu, Q. T.; Li, J. C.; Xue, H. G.; Guo, S. P. Binary iron sulfides as anode materials for rechargeable batteries: Crystal structures, syntheses, and electrochemical performance. *J. Power Sources*, 2018, 379: 41–52.

[36] Xu, J.; Avellan, A.; Li, H.; Liu, X. T.; Noël, V.; Lou, Z. M.; Wang, Y.; Kaegi, R.; Henkelman, G.; Lowry, G. V. Sulfur loading and speciation control the hydrophobicity, electron transfer, reactivity, and selectivity of sulfidized nanoscale zerovalent iron. *Adv. Mater.*, 2020, 32: 1906910.

[37] Liu, Z. C.; Chen, L.; Song, Y. R.; Zhong, Y.; Chen, Z. J.; Zhang, X. T.; Wang, X. M. Highly efficient PMS activation by synergistic effects of FeS_2/CoS_2 for rapid diuron degradation: Advanced oxidation and mechanism. *Environ. Res.*, 2025, 270: 121015.

[38] Wu, R.; Zheng, Y. F.; Zhang, X. G.; Sun, Y. F.; Xu, J. B.; Jian, J. K. Hydrothermal synthesis and crystal structure of pyrite. *J. Cryst. Growth*, 2004, 266: 523–527.

[39] Schmøkel, M. S.; Bjerg, L.; Cenedese, S.; Jørgensen, M. R. V.; Chen, Y. S.; Overgaard, J.; Iversen, B. B. Atomic properties and chemical bonding in the pyrite and marcasite polymorphs of FeS_2: A combined experimental and theoretical electron density study. *Chem. Sci.*, 2014, 5: 1408–1421.

[40] Wang, Y. J.; Chen, J.; Gao, J. X.; Meng, H. S.; Chai, S. N.; Jian, Y. F.; Shi, L. M.; Wang, Y. B.; He, C. Selective electrochemical H_2O_2 generation on the graphene aerogel for efficient electro-Fenton degradation of ciprofloxacin. *Sep. Purif. Technol.*, 2021, 272: 118884.

[41] Walkowiak, A.; Wolski, L.; Ziolek, M. The influence of ferrocene anchoring method on the reactivity and stability of SBA-15-based catalysts in the degradation of ciprofloxacin *via* photo-Fenton process. *RSC Adv.*, 2023, 13: 8360–8373.

[42] Nie, X.; Li, G. Y.; Li, S. S.; Luo, Y. M.; Luo, W. M.; Wan, Q.; An, T. C. Highly efficient adsorption and catalytic degradation of ciprofloxacin by a novel heterogeneous Fenton catalyst of hexapod-like pyrite nanosheets mineral clusters. *Appl. Catal. B Environ.*, 2022, 300: 120734.

[43] Liu, H. Y.; Shao, Y. H.; Dou, S.; Pan, C. S. Enhanced photo-Fenton degradation of antibiotics through internal electric field formation at the interface of mixed-phase FeS_2. *Sci. Energy Environ.*, 2024, 9.

[44] Pothu, R.; Bolagam, R.; Wang, Q. H.; Ni, W.; Cai, J. F.; Peng, X. X.; Feng, Y. Z.; Ma, J. M. Nickel sulfide-based energy storage materials for high-performance electrochemical capacitors. *Rare Met.*, 2021, 40: 353–373.

[45] Jiang, N.; Tang, Q.; Sheng, M. L.; You, B.; Jiang, D. E.; Sun, Y. J. Nickel sulfides for electrocatalytic hydrogen evolution under alkaline conditions: A case study of crystalline NiS, NiS_2, and Ni3S2 nanoparticles. *Catal. Sci. Technol.*, 2016, 6: 1077–1084.

[46] Haider, S.; Shar, S. S.; Shakir, I.; Agboola, P. O. Design of NiS/CNTs nanocomposites for visible light driven catalysis and antibacterial activity studies. *Ceram. Int.*, 2021, 47: 34269–34277.

[47] Fatima, R.; Warsi, M. F.; Zulfiqar, S.; Ragab, S. A.; Shakir, I.; Sarwar, M. I. Nanocrystalline transition metal oxides and their composites with reduced graphene oxide and carbon nanotubes for photocatalytic applications. *Ceram. Int.*, 2020, 46: 16480–16492.

[48] Sun, Y. J.; Liu, C.; Grauer, D. C.; Yano, J.; Long, J. R.; Yang, P. D.; Chang, C. J. Electrodeposited cobalt-sulfide catalyst for electrochemical and photoelectrochemical hydrogen generation from water. *J. Am. Chem. Soc.*, 2013, 135(47): 17699–17702.

[49] Liu, W. J.; Kwon, E.; Thanh, B. X.; Khiem, T. C.; Lisak, G.; Lee, J.; Lin, K. A. 3D hexagonal hierachitectured cobalt sulfide as an enhanced catalyst for activating monopersulfate to degrade sunscreen agent ensulizole. *J. Taiwan Inst. Chem. Eng.*, 2022, 131: 104109.

[50] Duan, X. M.; Xu, K. K.; Zhang, M. Z.; Xia, Y. Y.; Wang, L. P.; Chen, B. B.; Wang, C. C.; Wei, S. H.; Zhou, L. Crystal form-dependent MnS for diabetic wound healing: Performance and mechanistic insights. *Small*, 2024, 20: 2402496.

[51] Warrinnier, R.; Bossuyt, S.; Resseguier, C.; Cambier, P.; Houot, S.; Gustafsson, J. P.; Diels, J.; Smolders, E. Anaerobic respiration in the unsaturated zone of agricultural soil mobilizes phosphorus and manganese. *Environ. Sci. Technol.*, 2020, 54: 4922–4931.

[52] Howsawkeng, J.; Teel, A. L.; Hess, T. F.; Crawford, R. L.; Watts, R. J. Simultaneous abiotic reduction–biotic oxidation in a microbial-MnO_2-catalyzed Fenton-like system. *Sci. Total Environ.*, 2010, 409: 439–445.

[53] Liao, X. P.; Cao, J. R.; Lei, M.; Zhang, C. X.; Hu, L. S. Impact of manganese sulfide (*MnS*) oxygenation-induced oxidization on aqueous organic contaminants: Insight into the role of the hydroxyl radical (*HO·*). *Sci. Total Environ.*, 2022, 840: 156702.

[54] Sarkar, N.; Mishra, S. R.; Gadore, V.; Panigrahi, B.; Ahmaruzzaman, M. Nanocosmos of catalysis: A voyage through synthesis, properties, and enhanced photocatalytic degradation in nickel sulfide nanocomposites. *Nanoscale Adv.*, 2024, 6: 2741–2765.

[55] Liu, L.; Li, Y. T.; Jiang, X. L.; Zhang, Z. J.; Ma, L. F.; Li, T.; Yang, G. L. Adsorption of CO and SO_2 on SnS monolayer doped with transition metal oxides (TiO_2, CuO, and NiO): A DFT study. *Mater. Sci. Semicond. Process.*, 2024, 181: 108644.

[56] Jameel, M. H.; bin Roslan, M. S.; Mayzan, M. Z. H. B.; Shaaban, I. A.; Rizvi, S. Z. H.; Agam, M. A. B.; Saleem, S.; Assiri, M. A. A comparative DFT study of bandgap engineering and tuning of structural, electronic, and optical properties of 2D WS_2, PtS2, and MoS_2 between WSe_2, PtSe2, and $MoSe_2$ materials for photocatalytic and solar cell applications. *J. Inorg. Organomet. Polym. Mater.*, 2024, 34: 322–335.

[57] Oh, W. D.; Lim, T. T. Design and application of heterogeneous catalysts as peroxydisulfate activator for organics removal: An overview. *Chem. Eng. J.*, 2019, 358: 110–133.

[58] Dou, J. B.; Su, X.; Wu, J. X.; Li, S. Y.; Dai, H. Y.; Liu, M.; Tang, Y.; Lu, Z. J.; Xu, J. M.; He, Y. Peroxydisulfate-driven reductive dechlorination as affected by soil constituents: Free radical formation and conversion. *Environ. Sci. Technol.*, 2024, 58(18): 8065–8075.

[59] Lee, J.; von Gunten, U.; Kim, J. H. Persulfate-based advanced oxidation: Critical assessment of opportunities and roadblocks. *Environ. Sci. Technol.*, 2020, 54(6): 3064–3081.

[60] Ding, Y. B.; Wang, X. R.; Fu, L. B.; Peng, X. Q.; Pan, C.; Mao, Q. H.; Wang, C. J.; Yan, J. C. Nonradicals induced degradation of organic pollutants by peroxydisulfate (PDS) and peroxymonosulfate (PMS): Recent advances and perspective. *Sci. Total Environ.*, 2021, 765: 142794.

[61] Yin, W. Z.; Yang, B.; Fu, Y. F.; Chu, F. D.; Yao, J.; Cao, S. H.; Zhu, Z. L. Effect of calcium hypochlorite on flotation separation of covellite and pyrite. *Powder Technol.*, 2019, 343: 578–585.

[62] Qin, W. X.; Fang, G. D.; Wang, Y. J.; Zhou, D. M. Mechanistic understanding of polychlorinated biphenyls degradation by peroxymonosulfate activated with $CuFe_2O_4$ nanoparticles: Key role of superoxide radicals. *Chem. Eng. J.*, 2018, 348: 526–534.

[63] Ding, Y. B.; Zhu, L. H.; Wang, N.; Tang, H. Q. Sulfate radicals induced degradation of tetrabromobisphenol A with nanoscaled magnetic $CuFe_2O_4$ as a heterogeneous catalyst of peroxymonosulfate. *Appl. Catal. B Environ.*, 2013, 129: 153–162.

[64] Wang, Y. B.; Zhao, H. Y.; Li, M. F.; Fan, J. Q.; Zhao, G. H. Magnetic ordered mesoporous copper ferrite as a heterogeneous Fenton catalyst for the degradation of imidacloprid. *Appl. Catal. B* 2014, *147*: 534-545.

[65] Peng, J. L.; Lu, X. H.; Jiang, X.; Zhang, Y. H.; Chen, Q. X.; Lai, B.; Yao, G. Degradation of atrazine by persulfate activation with copper sulfide (CuS): Kinetics study, degradation pathways and mechanism. *Chem. Eng. J.* 2018, *354*: 740-752.

[66] Wang, X. L.; Ding, Y. Z.; Dionysiou, D. D.; Liu, C.; Tong, Y. P.; Gao, J.; Fang, G. D.; Zhou, D. M. Efficient activation of peroxymonosulfate by copper sulfide for diethyl phthalate degradation: Performance, radical generation and mechanism. *Sci. Total Environ.* 2020, *749*: 142387.

[67] Jeong, H. Y.; Lee, J. H.; Hayes, K. F. Characterization of synthetic nanocrystalline mackinawite: crystal structure, particle size, and specific surface area. *Geochim. Cosmochim. Acta* 2008, *72* (2): 493-505.

[68] Sun, Y.; Danish, M.; Ali, M.; Shan, A.; Li, M.; Lyu, Y. C.; Qiu, Z. F.; Sui, Q.; Zang, X. K.; Lyu, S. G. Trichloroethene degradation by nanoscale CaO_2 activated with Fe (II)/FeS: the role of FeS and the synergistic activation mechanism of Fe (II)/FeS. *Chem. Eng. J.* 2020, *394*: 124830.

[69] Fan, J. H.; Gu, L.; Wu, D. L.; Liu, Z. G. Mackinawite (FeS) activation of persulfate for the degradation of p-chloroaniline: surface reaction mechanism and sulfur-mediated cycling of iron species. *Chem. Eng. J.* 2018, *333*: 657-664.

[70] Yang, S. R.; He, C. S.; Xie, Z. H.; Li, L. L.; Xiong, Z. K.; Zhang, H.; Zhou, P.; Jiang, F.; Mu, Y.; Lai, B. Efficient activation of PAA by FeS for fast removal of pharmaceuticals: The dual role of sulfur species in regulating the reactive oxidized species. *Water Res.* 2022, *217*: 118402.

[71] Luo, C. W.; Jiang, L.; Li, X. F.; Wan, Q. M.; Jiang, T. J.; Mao, S. P.; Guo, J. Q.; Zhao, R. Z.; Xie, C. Enhanced activation of peroxymonosulfate by nickel sulfide with sulfur vacancies for ultrafast organic pollutants degradation: Roles of active sites and mechanism. *Environ. Pollut.* 2025, *372*: 125789.

[72] Zhu, Z. L.; Yan, J. B.; Wang, M. X.; Zhu, H.; Li, X. K.; Wu, L. Insights into hydrangea-like $NiCo_2S_4$ activating peroxymonosulfate for efficient degradation of atrazine. *Chem. Eng. J.*, 2023, 477: 146876.

[73] Lyu, C.; Zhang, L.; He, D.; Su, B. Y.; Lyu, Y. Micrometer-sized NiOOH hierarchical spheres for enhanced degradation of sulfadiazine *via* synergistic adsorption and catalytic oxidation in peroxymonosulfate system. *Chin. Chem. Lett.*, 2022, 33: 930–934.

[74] Yan, C. C.; Li, J.; Sun, Z. H.; Chen, L. Y.; Sun, X.; Wang, X. J.; Xia, S. Q. Engineering sulfur vacancies on Mo-doped FeS_2 nanosheets grown on activated carbon fibers enhances peroxymonosulfate activation for efficient elimination of sulfamethazine, antibiotic resistant bacteria and antibiotic resistance genes: The dominant role of singlet oxygen. *Chem. Eng. J.*, 2024, 493: 152643.

[75] Xu, S. Z.; Wang, P. F.; Mi, X. Y.; Bao, Y. P.; Zhang, H.; Mo, F.; Zhou, Q. X.; Zhan, S. H. N, S, and Cl tri-doped carbon boost the switching of radical to non-radical pathway in Fenton-like reactions: Synergism of N species and defects. *J. Hazard. Mater.*, 2024, 466: 133321.

[76] Wu, Y.; Xing, Y. Y.; Zhao, X. D.; Zhou, Z. M.; Jing, G. H. Mechanistic insights into rapid sulfite activation with cobalt sulfide towards iohexol abatement: Contribution of sulfur conversion. *Chem. Eng. J.*, 2022, 429: 132404.

[77] Chen, Y. Q.; Ruan, J. D.; Zeng, B. T.; Jiang, W.; Luo, L. T.; Shao, Q.; Liu, Z. Z. Insights into the sulfite activation by cobalt (II) sulfide for acetaminophen removal: A synergistic catalysis and DFT calculations. J. Environ. *Chem. Eng.* 2022, *10* (3): 107709.

[78] Li, C. X.; Wu, J. E.; Peng, W.; Fang, Z. D.; Liu, J. Peroxymonosulfate activation for efficient sulfamethoxazole degradation by Fe_3O_4/β-FeOOH nanocomposites: Coexistence of radical and non-radical reactions. *Chem. Eng. J.*, 2019, 356: 904–914.

[79] Li, W. Q.; Li, S. Q.; Tang, Y.; Yang, X. L.; Zhang, W. X.; Zhang, X. D.; Chai, H. X.; Huang, Y. M. Highly efficient activation of peroxymonosulfate by cobalt sulfide hollow nanospheres for fast ciprofloxacin degradation. *J. Hazard. Mater.*, 2020, 389: 121856.

[80] Zhang, S. H.; Lv, J. T.; Han, R. X.; Wang, Z.; Christie, P.; Zhang, S. Z. Sustained production of superoxide radicals by manganese oxides under ambient dark conditions. *Water Res.*, 2021, 196: 117034.

[81] Gao, Y.; Jiang, J.; Zhou, Y.; Pang, S. Y.; Jiang, C. C.; Guo, Q.; Duan, J. B. Does soluble Mn(III) oxidant formed *in situ* account for enhanced transformation of triclosan by Mn(VII) in the presence of ligands. *Environ. Sci. Technol.*, 2018, 52(8): 4785–4793.

[82] Rao, D. D.; Dong, H. Y.; Lian, L. S.; Sun, Y. K.; Zhang, X.; Dong, L.; Zhou, G. M.; Guan, X. H. New mechanistic insights into the transformation of reactive oxidizing species in an ultraviolet/sulfite system under aerobic conditions: Modeling and the impact of Mn(II). *ACS EST Water*, 2021, 1(8): 1785–1795.

[83] Zhang, J. M.; Ma, J.; Song, H. R.; Sun, S. F.; Zhang, Z. X.; Yang, T. Organic contaminants degradation from the S(IV) autoxidation process catalyzed by ferrous-manganous ions: A noticeable Mn(III) oxidation process. *Water Res.*, 2018, 133: 227–235.

[84] Rao, D. D.; Sun, Y. K.; Shao, B. B.; Qiao, J. L.; Guan, X. H. Activation of oxygen with sulfite for enhanced Removal of Mn(II): The involvement of $SO_4^{\bullet-}$. *Water Res.*, 2019, 157: 435–444.

[85] Ge, C.; Wang, X. H.; Yu, F. R.; Chen, H.; Fang, G. D.; Wang, Y. J.; Gao, J. Mechanistic insight into manganese oxidation induced

by sulfite under aerobic condition: Implication of triclosan degradation. *Sep. Purif. Technol.*, 2023, 306: 122583.

[86] Zhang, P.; Huang, W.; Ji, Z.; Zhou, C. G.; Yuan, S. H. Mechanisms of hydroxyl radicals production from pyrite oxidation by hydrogen peroxide: Surface versus aqueous reactions. *Geochim. Cosmochim. Acta*, 2018, 238: 394–410.

[87] Song, B.; Zeng, Z. T.; Almatrafi, E.; Shen, M. C.; Xiong, W. P.; Zhou, C. Y.; Wang, W. J.; Zeng, G. M.; Gong, J. L. Pyrite-mediated advanced oxidation processes: Applications, mechanisms, and enhancing strategies. *Water Res.*, 2022, 211: 118048.

[88] Rahimi, F.; van der Hoek, J. P.; Royer, S.; Javid, A.; Mashayekh-Salehi, A.; Jafari Sani, M. Pyrite nanoparticles derived from mine waste as efficient catalyst for the activation of persulfates for degradation of tetracycline. *J. Water Process. Eng.*, 2021, 40: 101808.

[89] Ismail, L.; Ferronato, C.; Fine, L.; Jaber, F.; Chovelon, J. M. Elimination of sulfaclozine from water with SO_4^- radicals: Evaluation of different persulfate activation methods. *Appl. Catal. B Environ.*, 2017, 201: 573–581.

[90] He, P.; Zhu, J. Y.; Chen, Y. Z.; Chen, F.; Zhu, J. L.; Liu, M. F.; Zhang, K.; Gan, M. Pyrite-activated persulfate for simultaneous 2, 4-DCP oxidation and Cr(VI) reduction. *Chem. Eng. J.*, 2021, 406: 126758.

[91] Zhou, H. Y.; Lai, L. D.; Wan, Y. J.; He, Y. L.; Yao, G.; Lai, B. Molybdenum disulfide (MoS_2): A versatile activator of both peroxymonosulfate and persulfate for the degradation of carbamazepine. *Chem. Eng. J.*, 2020, 384: 123264.

[92] Chen, Y.; Zhang, G.; Liu, H. J.; Qu, J. H. Confining free radicals in close vicinity to contaminants enables ultrafast Fenton-like processes in the interspacing of MoS_2 membranes. *Angew. Chem. Int. Ed.*, 2019, 58: 8134–8138.

[93] Zhao, L.; Liu, L.; Bai, X. F.; Zhang, A. Y.; Peng, S. C.; Zhang, C.; Niu, H. H.; Liang, H. Defect-tailored MoS_2 for superior Fenton-like catalysis: The synergistic reactive sites of 1T phase and sulfur vacancy in electron transfer and radical generation. *Sep. Purif. Technol.*, 2023, 318: 123997.

[94] Yin, Y.; Shi, L.; Li, W. L.; Li, X. N.; Wu, H.; Ao, Z. M.; Tian, W. J.; Liu, S. M.; Wang, S. B.; Sun, H. Q. Boosting Fenton-like reactions *via* single atom Fe catalysis. *Environ. Sci. Technol.*, 2019, 53(19): 11391–11400.

[95] Liu, J. Y.; Hu, Y. Y.; Li, X.; Xiao, C.; Yuan, B. W.; Cheng, J. H.; Chen, Y. C.; Zhu, X. Q.; Wang, G. B.; Xie, J. Y. Efficient simultaneous removal enrofloxacin and Cr(VI) *via* activation of peroxymonosulfate over defect-rich C-MoS_2-Fe. *Appl. Catal. B Environ. Energy*, 2024, 348: 123818.

[96] Sun, Y. B.; Zhou, Y.; Li, H. C.; Wang, C.; Zhang, X.; Ma, Q.; Cheng, Y. C.; Qian, J. S.; Pan, B. C. Confinement of Fe atoms between MoS_2 interlayers drives phase transition for improved reactivity in Fenton-like reactions. *Nano Res.*, 2024, 17: 1132–1139.

[97] Sun, T.; Su, Y. Y.; Song, H. J.; Lv, Y. New advanced oxidation progress with chemiluminescence behavior based on NaClO triggered by WS_2 nanosheets. *J. Hazard. Mater.*, 2022, 429: 128329.

[98] Zhou, H. Y.; Zhang, H.; He, Y. L.; Huang, B. K.; Zhou, C. Y.; Yao, G.; Lai, B. Critical review of reductant-enhanced peroxide activation processes: Trade-off between accelerated Fe^{3+}/Fe^{2+} cycle and quenching reactions. *Appl. Catal. B Environ.*, 2021, 286: 119900.

[99] Xing, M. Y.; Xu, W. J.; Dong, C. C.; Bai, Y. C.; Zeng, J. B.; Zhou, Y.; Zhang, J. L.; Yin, Y. D. Metal sulfides as excellent co-catalysts for H_2O_2 decomposition in advanced oxidation processes. *Chem*, 2018, 4: 1359–1372.

[100] Li, Y. J.; Dong, H. R.; Li, L.; Tang, L.; Tian, R.; Li, R.; Chen, J.; Xie, Q. Q.; Jin, Z. L.; Xiao, J. Y. et al. Recent advances in waste water treatment through transition metal sulfides-based advanced oxidation processes. *Water Res.*, 2021, 192: 116850.

[101] Ao, X. W.; Eloranta, J.; Huang, C. H.; Santoro, D.; Sun, W. J.; Lu, Z. D.; Li, C. Peracetic acid-based advanced oxidation processes for decontamination and disinfection of water: A review. *Water Res.*, 2021, 188: 116479.

[102] Wang, P. X.; He, X.; Zhang, W.; Ma, J.; Jiang, J.; Huang, Z. S.; Cheng, H. J.; Pang, S. Y.; Zhou, Y.; Zhai, X. D. Highly efficient removal of p-arsanilic acid with Fe(II)/peroxydisulfate under near-neutral conditions. *Water Res.*, 2020, 177: 115752.

[103] Fan, Y.; Ji, Y. F.; Kong, D. Y.; Lu, J. H.; Zhou, Q. S. Kinetic and mechanistic investigations of the degradation of sulfamethazine in heat-activated persulfate oxidation process. *J. Hazard. Mater.*, 2015, 300: 39–47.

[104] Furman, O. S.; Teel, A. L.; Watts, R. J. Mechanism of base activation of persulfate. *Environ. Sci. Technol.*, 2010, 44(16): 6423–6428.

[105] Gao, Y. Q.; Gao, N. Y.; Chu, W. H.; Zhang, Y. F.; Zhang, J.; Yin, D. Q. UV-activated persulfate oxidation of sulfamethoxypyridazine: Kinetics, degradation pathways and impact on DBP formation during subsequent chlorination. *Chem. Eng. J.*, 2019, 370: 706–715.

[106] Liu, J. W.; Peng, C. S.; Shi, X. L. Preparation, characterization, and applications of Fe-based catalysts in advanced oxidation processes for organics removal: A review. *Environ. Pollut.*, 2022, 293: 118565.

[107] Yan, Y. Q.; Wei, Z. S.; Duan, X. G.; Long, M. C.; Spinney, R.; Dionysiou, D. D.; Xiao, R. Y.; Alvarez, P. J. J. Merits and limitations of radical *vs.* nonradical pathways in persulfate-based advanced oxidation processes. *Environ. Sci. Technol.*, 2023, 57(33): 12153–12179.

[108] Norzaee, S.; Taghavi, M.; Djahed, B.; Kord Mostafapour, F. Degradation of Penicillin G by heat activated persulfate in aqueous solution. *J. Environ. Manag.*, 2018, 215: 316–323.

[109] Guerra-Rodríguez, S.; Rodríguez, E.; Singh, D. N.; Rodríguez-Chueca, J. Assessment of sulfate radical-based advanced oxidation processes for water and wastewater treatment: A review. *Water*, 2018, 10: 1828.

[110] Duan, X. G.; Ao, Z. M.; Sun, H. Q.; Indrawirawan, S.; Wang, Y. X.; Kang, J.; Liang, F. L.; Zhu, Z. H.; Wang, S. B. Nitrogen-doped graphene for generation and evolution of reactive radicals by metal-free catalysis. *ACS Appl. Mater. Interfaces*, 2015, 7(7): 4169–4178.

[111] Duan, X. G.; Sun, H. Q.; Wang, S. B. Metal-free carbocatalysis in advanced oxidation reactions. *Acc. Chem. Res.*, 2018, 51(3): 678–687.

[112] Hayat, W.; Zhang, Y. Q.; Hussain, I.; Huang, S. B.; Du, X. D. Comparison of radical and non-radical activated persulfate systems for the degradation of imidacloprid in water. *Ecotoxicol. Environ. Saf.*, 2020, 188: 109891.

[113] Wang, J. L.; Wang, S. Z. Effect of inorganic anions on the performance of advanced oxidation processes for degradation of organic contaminants. *Chem. Eng. J.*, 2021, 411: 128392.

[114] Liu, H.; Dai, X. H.; Kong, L. S.; Sui, C. J.; Nie, Z. X.; Liu, Y.; Cai, B.; Ni, S. Q.; Boczkaj, G.; Zhan, J. H. Ball milling treatment of Mn_3O_4 regulates electron transfer pathway for peroxymonosulfate activation. *Chem. Eng. J.*, 2023, 467: 143339.

[115] Chen, H.; Zhang, Z. L.; Feng, M. B.; Liu, W.; Wang, W. J.; Yang, Q.; Hu, Y. A. Degradation of 2, 4-dichlorophenoxyacetic acid in water by persulfate activated with FeS (mackinawite). *Chem. Eng. J.*, 2017, 313: 498–507.

[116] Qi, C. D.; Liu, X. T.; Lin, C. Y.; Zhang, X. H.; Ma, J.; Tan, H. B.; Ye, W. Degradation of sulfamethoxazole by microwave-activated persulfate: Kinetics, mechanism and acute toxicity. *Chem. Eng. J.*, 2014, 249: 6–14.

[117] Vicente, F.; Santos, A.; Romero, A.; Rodriguez, S. Kinetic study of diuron oxidation and mineralization by persulphate: Effects of

temperature, oxidant concentration and iron dosage method. *Chem. Eng. J.*, 2011, 170: 127–135.

[118] Zhou, T.; Zou, X. L.; Mao, J.; Wu, X. H. Decomposition of sulfadiazine in a sonochemical Fe^0-catalyzed persulfate system: Parameters optimizing and interferences of wastewater matrix. *Appl. Catal. B Environ.*, 2016, 185: 31–41.

[119] Xu, Y.; Lin, H.; Li, Y. K.; Zhang, H. The mechanism and efficiency of MnO_2 activated persulfate process coupled with electrolysis. *Sci. Total Environ.*, 2017, 609: 644–654.

[120] Lamsal, R.; Walsh, M. E.; Gagnon, G. A. Comparison of advanced oxidation processes for the removal of natural organic matter. *Water Res.*, 2011, 45: 3263–3269.

[121] Gao, H. P.; Chen, J. B.; Zhang, Y. L.; Zhou, X. F. Sulfate radicals induced degradation of Triclosan in thermally activated persulfate system. *Chem. Eng. J.*, 2016, 306: 522–530.

[122] Nie, M. H.; Yang, Y.; Zhang, Z. J.; Yan, C. X.; Wang, X. N.; Li, H. J.; Dong, W. B. Degradation of chloramphenicol by thermally activated persulfate in aqueous solution. *Chem. Eng. J.*, 2014, 246: 373–382.

[123] Feng, Y. P.; Song, Q. Y.; Lv, W. Y.; Liu, G. G. Degradation of ketoprofen by sulfate radical-based advanced oxidation processes: Kinetics, mechanisms, and effects of natural water matrices. *Chemosphere*, 2017, 189: 643–651.

[124] Zhao, W. Q.; Yuan, S. H.; Zhang, L. M.; Jiang, F.; Yang, Y.; Zou, G. Q.; Hou, H. S.; Ge, P.; Sun, W.; Ji, X. B. Engineering metal-sulfides with cations-tunable metal-oxides electrocatalysts with promoted catalytic conversion for robust ions-storage capability. *Energy Storage Mater.*, 2022, 45: 1183–1200.

[125] Lim, D.; Min, K.; Hwang, M.; Ham, H. C.; Kim, G. J.; Baeck, S. H. Hollow hierarchical zinc cobalt sulfides derived from bimetallic-organic-framework as a non-precious electrocatalyst for oxygen reduction reaction. *Mol. Catal.*, 2021, 509: 111614.

[126] Yang, H. Y.; Guo, P. F.; Wang, R. R.; Chen, Z. L.; Xu, H. B.; Pan, H. G.; Sun, D. L.; Fang, F.; Wu, R. B. Sequential phase conversion-induced phosphides heteronanorod arrays for superior hydrogen evolution performance to Pt in wide pH media. *Adv. Mater.*, 2022, 34: 2107548.

[127] Zhao, X. H.; Xue, Z. M.; Chen, W. J.; Wang, Y. Q.; Mu, T. C. Eutectic synthesis of high-entropy metal phosphides for electrocatalytic water splitting. *ChemSusChem*, 2020, 13: 2038–2042.

[128] Liu, Y. K.; Jiang, S.; Li, S. J.; Zhou, L.; Li, Z. H.; Li, J. M.; Shao, M. F. Interface engineering of (Ni, Fe)S_2@MoS_2 heterostructures for synergetic electrochemical water splitting. *Appl. Catal. B Environ.*, 2019, 247: 107–114.

[129] Chen, J. N.; Yuan, X. L.; Lyu, F. L.; Zhong, Q. X.; Hu, H. C.; Pan, Q.; Zhang, Q. Integrating MXene nanosheets with cobalt-tipped carbon nanotubes for an efficient oxygen reduction reaction. *J. Mater. Chem. A*, 2019, 7: 1281–1286.

[130] Xiao, S. S.; Zhang, Y. C.; Zhou, X. G.; Li, Y. Q.; Lin, N.; Wang, Q. L.; Bi, F.; Zhao, L.; Wang, L. Y. Bimetallic sulfides based hybrid anodes are constructed for high-performance lithium ion batteries. *Talanta*, 2025, 285: 127343.

[131] Ma, B.; Chen, T. T.; Li, Q. Y.; Qin, H. N.; Dong, X. Y.; Zang, S. Q. Bimetal–organic-framework-derived nanohybrids $Cu_{0.9}Co_{2.1}S_4$@MoS_2 for high-performance visible-light-catalytic hydrogen evolution reaction. *ACS Appl. Energy Mater.*, 2019, 2: 1134–1148.

[132] Ye, L. W.; Yuan, Y. F.; Wang, L. N.; Zhu, M.; Yin, S. M.; Chen, Y. B.; Guo, S. Y. $NiCo_2S_4$/Co_3S_4 heterogeneous double-shelled nanocages for high-performance electrochemical energy storage. *Mater. Lett.*, 2018, 229: 152–155.

[133] An, K.; Kwon, S. G.; Park, M.; Na, H. B.; Baik, S. I.; Yu, J. H.; Kim, D.; Son, J. S.; Kim, Y. W.; Song, I. C. et al. Synthesis of uniform hollow oxide nanoparticles through nanoscale acid etching. *Nano Lett.*, 2008, 8(12): 4252–4258.

[134] Shao, P. H.; Tian, J. Y.; Duan, X. G.; Yang, Y.; Shi, W. X.; Luo, X. B.; Cui, F. Y.; Luo, S. L.; Wang, S. B. Cobalt silicate hydroxide nanosheets in hierarchical hollow architecture with maximized cobalt active site for catalytic oxidation. *Chem. Eng. J.*, 2019, 359: 79–87.

[135] Qi, H. Y.; Zhong, J. D.; Sun, W. B.; Xu, T. T.; Xing, Z.; Zhao, S.; Qian, H. J.; Zhang, H. B.; Mu, J. X.; Zhu, X. B. et al. Integrated device for osmotic energy collection and detection based on the metal–organic framework of nanoconfinement channels. *CCS Chem.*, 2025, 7: 1424–1437.

[136] Yaghi, O. M.; Li, H. L. Hydrothermal synthesis of a metal-organic framework containing large rectangular channels. *J. Am. Chem. Soc.*, 1995, 117(41): 10401–10402.

[137] Li, H. L.; Eddaoudi, M.; O'Keeffe, M.; Yaghi, O. M. Design and synthesis of an exceptionally stable and highly porous metal-organic framework. *Nature*, 1999, 402: 276–279.

[138] Furukawa, H.; Cordova, K. E.; O'Keeffe, M.; Yaghi, O. M. The chemistry and applications of metal-organic frameworks. *Science*, 2013, 341: 1230444.

[139] Xia, W.; Mahmood, A.; Zou, R. Q.; Xu, Q. Metal–organic frameworks and their derived nanostructures for electrochemical energy storage and conversion. *Energy Environ. Sci.*, 2015, 8: 1837–1866.

[140] Xiong, Z. K.; Jiang, Y. N.; Wu, Z. L.; Yao, G.; Lai, B. Synthesis strategies and emerging mechanisms of metal-organic frameworks for sulfate radical-based advanced oxidation process: A review. *Chem. Eng. J.*, 2021, 421: 127863.

[141] Gu, Z. Y.; Park, J.; Raiff, A.; Wei, Z. W.; Zhou, H. C. Metal–organic frameworks as biomimetic catalysts. *ChemCatChem*, 2014, 6: 67–75.

[142] Liang, P.; Wang, Q. C.; Kang, J.; Tian, W. J.; Sun, H. Q.; Wang, S. B. Dual-metal zeolitic imidazolate frameworks and their derived nanoporous carbons for multiple environmental and electrochemical applications. *Chem. Eng. J.*, 2018, 351: 641–649.

[143] Jiang, H.; Zhu, C. Q.; Yuan, Y.; Yue, C. L.; Ling, C.; Liu, F. Q.; Li, A. M. Enhanced activation of peroxymonosulfate with metal-substituted hollow $M_xCo_{3-x}S_4$ polyhedrons for superfast degradation of sulfamethazine. *Chem. Eng. J.*, 2020, 384: 123302.

[144] Li, J.; Ni, Z. B.; Gao, Q. Z.; Yang, X. X.; Fang, Y. P.; Qiu, R. L.; Zhu, M. S.; Zhang, S. S. Core-shell structured cobalt–nickel bimetallic sulfide with dual redox cycles to activate peroxymonosulfate for glyphosate removal. *Chem. Eng. J.*, 2023, 453: 139972.

[145] Luo, X. H.; Zhou, Q. L.; Du, S.; Li, J.; Zhang, L.; Lin, K. D.; Li, H.; Chen, B.; Wu, T.; Chen, D. C. et al. One-dimensional porous hybrid structure of Mo2C-CoP encapsulated in N-doped carbon derived from MOF: An efficient electrocatalyst for hydrogen evolution reaction over the entire pH range. *ACS Appl. Mater. Interfaces*, 2018, 10(49): 42335–42347.

[146] Wang, T.; Jin, R. M.; Wu, X. Q.; Zheng, J.; Li, X. G.; Ostrikov, K. A highly efficient Ni–Mo bimetallic hydrogen evolution catalyst derived from a molybdate incorporated Ni-MOF. *J. Mater. Chem. A*, 2018, 6: 9228–9235.

[147] Liu, P.; Yan, J. Y.; Mao, J. X.; Li, J. W.; Liang, D. X.; Song, W. B. In-plane intergrowth CoS_2/MoS_2 nanosheets: Binary metal–organic framework evolution and efficient alkaline HER electrocatalysis. *J. Mater. Chem. A*, 2020, 8: 11435–11441.

[148] Li, X.; Wang, X. L.; Zhou, J.; Han, L.; Sun, C. Y.; Wang, Q. Q.; Su, Z. M. Ternary hybrids as efficient bifunctional electrocatalysts derived from bimetallic metal–organic-frameworks for overall water splitting. *J. Mater. Chem. A*, 2018, 6: 5789–5796.

[149] Xie, J. F.; Zhang, H.; Li, S.; Wang, R. X.; Sun, X.; Zhou, M.; Zhou, J. F.; Lou, X. W.; Xie, Y. Defect-rich MoS_2 ultrathin nanosheets with additional active edge sites for enhanced electrocatalytic hydrogen evolution. *Adv. Mater.*, 2013, 25: 5807–5813.

[150] Lou, Y.; Zheng, Y. P.; Li, X.; Ta, N.; Xu, J.; Nie, Y. F.; Cho, K.; Liu, J. Y.

Pocketlike active site of Rh1/MoS_2 single-atom catalyst for selective crotonaldehyde hydrogenation. *J. Am. Chem. Soc.*, 2019, 141(49): 19289–19295.

[151] Li, Z. X.; Sun, M.; Yang, J. L.; Dong, S. S. High-performance iron-doped molybdenum disulfide photocatalysts enhance peroxymonosulfate activation for water decontamination. *Chem. Eng. J.*, 2022, 446: 137380.

[152] Xie, Q. Q.; Wang, X. X.; Chen, W. Q.; Lei, C.; Huang, B. B. Engineering active heterojunction architecture with oxygenated-Co, Mo bimetallic sulfide heteronanosheet and graphene oxide for peroxymonosulfate activation. *J. Hazard. Mater.*, 2023, 448: 130852.

[153] Wang, W.; Luo, Q.; Li, L. Q.; Chen, S. P.; Wang, Y. F.; Du, X. W.; Wang, N. Hybrid nickel-molybdenum bimetallic sulfide nanozymes for antibacterial and antibiofouling applications. *Adv. Compos. Hybrid Mater.*, 2023, 6: 139.

[154] Yang, K.; Zhai, Z. H.; Liu, H. L.; Zhao, T. T.; Yuan, D. L.; Jiao, T. F.; Zhang, Q. R.; Tang, S. F. Peracetic acid activation by natural chalcopyrite for metronidazole degradation: Unveiling the effects of Cu-Fe bimetallic sites and sulfur species. *Sep. Purif. Technol.*, 2023, 305: 122500.

[155] Fan, C. Y.; Zang, Z. H.; Zhang, X. H. Non-metal doping regulation in transition metal and their compounds for electrocatalytic water splitting. *Int. J. Hydrog. Energy*, 2024, 56: 1273–1283.

[156] Liu, Y.; Wang, W.; Xu, X. M.; Marcel Veder, J. P.; Shao, Z. P. Recent advances in anion-doped metal oxides for catalytic applications. *J. Mater. Chem. A*, 2019, 7: 7280–7300.

[157] Zhao, C. X.; Li, B. Q.; Zhao, M.; Liu, J. N.; Zhao, L. D.; Chen, X.; Zhang, Q. Precise anionic regulation of NiFe hydroxysulfide assisted by electrochemical reactions for efficient electrocatalysis. *Energy Environ. Sci.*, 2020, 13: 1711–1716.

[158] Kou, T. Y.; Smart, T.; Yao, B.; Chen, I.; Thota, D.; Ping, Y.; Li, Y. Theoretical and experimental insight into the effect of nitrogen doping on hydrogen evolution activity of Ni3S2 in alkaline medium. *Adv. Energy Mater.*, 2018, 8: 1703538.

[159] Cao, E. P.; Chen, Z. M.; Wu, H.; Yu, P.; Wang, Y.; Xiao, F.; Chen, S.; Du, S. C.; Xie, Y.; Wu, Y. Q. et al. Boron-induced electronic-structure reformation of CoP nanoparticles drives enhanced pH-universal hydrogen evolution. *Angew. Chem. Int. Ed.*, 2020, 59: 4154–4160.

[160] Shen, Y.; Yang, M. Z.; Zhu, C.; Zhang, H. Z.; Liu, R. L.; Wang, J.; Fang, Q. L.; Song, S.; Chen, B. L. Enhanced selectivity in PMS activation *via* non-metal doping for efficient $1O_2$ generation in emerging organic pollutants degradation. *ACS ES&T Engg.*, 2024, 4(11): 2839–2851.

[161] Wang, S. Q.; Yuan, T.; Lu, S. S.; Liu, Y. N.; Tang, Z. L.; Jiang, F.; Chen, H.; Cao, S. H. Construction of non-metal-doped carbon nitride and bismuth sulfide heterojunctions for effective degradation of bisphenol A: Promotion of directional transfer of photogenerated electrons. *J. Alloys Compd.*, 2025, 1036: 181811.

[162] Ye, J.; Zang, Y. P.; Wang, Q. Y.; Zhang, Y. D.; Sun, D.; Zhang, L. J.; Wang, G. M.; Zheng, X. S.; Zhu, J. F. Nitrogen doped FeS_2 nanoparticles for efficient and stable hydrogen evolution reaction. *J. Energy Chem.*, 2021, 56: 283–289.

[163] Zhou, S. F.; Yang, C. M.; Guo, L.; Ali Soomro, R.; Niu, M. M.; Yang, Z. X.; Du, R.; Wang, D. J.; Fu, F.; Xu, B. Synergism of electronic structure regulation and interface engineering for boosting hydrogen evolution reaction on S-Scheme FeS_2/S-$ZnSnO_3$ heterostructure. *Appl. Surf. Sci.*, 2023, 625: 157192.

[164] Luo, Y.; Zhang, Y. L.; Zhu, J. Y.; Tian, X. P.; Liu, G.; Feng, Z. M.; Pan, L. W.; Liu, X. H.; Han, N.; Tan, R. Material engineering strategies for efficient hydrogen evolution reaction catalysts. *Small Meth.*, 2024, 8: 2400158.

[165] Shi, J. J.; Chen, T.; Sun, X. L. The effect of heteroatom doping on the active metal site of CoS_2 for hydrogen evolution reaction. *RSC Adv.*, 2022, 12: 17257–17263.

[166] Lv, J. J.; Li, Y. L.; Wu, S. J.; Fang, H.; Li, L. L.; Song, R. B.; Ma, J.; Zhu, J. J. Oxygen species on nitrogen-doped carbon nanosheets as efficient active sites for multiple electrocatalysis. *ACS Appl. Mater. Interfaces*, 2018, 10(14): 11678–11688.

[167] Zhao, H.; Ren, J. T.; Yuan, Z. Y. Microenvironment engineering of gas-involving energy electrocatalysis and device applications. *Coord. Chem. Rev.*, 2024, 514: 215901.

[168] Tian, J. Y.; Yang, C. D.; Hao, R. H.; Li, F. N.; Liu, Z. R.; Chen, W.; Lv, Y. C.; Lin, C. Fabrication of phosphorus-mediated MoS_2 nanosheets on carbon cloth for enhanced hydrogen evolution reaction. *Int. J. Hydrog. Energy*, 2022, 47: 17871–17878.

[169] Xu, S. Y.; Chi, J. Q.; Cui, T.; Li, Z. P.; Liu, F. S.; Lai, J. P.; Wang, L. Substitutional phosphorus doping stimulates strong metal-support interactions for anion exchange membrane based alkaline seawater electrolysis. *Nano Energy*, 2024, 126: 109698.

[170] Fan, Y. Y.; Sun, Y. F.; Zhang, X.; Guo, J. X. Synergistic effect between sulfur and CoFe alloys embedded in N-doped carbon nanosheets for efficient hydrogen evolution under neutral condition. *Chem. Eng. J.*, 2021, 426: 131922.

[171] Wang, J. P.; Yao, J.; Li, Y. B.; Wei, Z. L.; Gao, C. Y.; Jiang, L. S.; Wu, X. Y. S vacancies-introduced chalcopyrite switch radical to non-radical pathways *via* peroxymonosulfate activation: Vital roles of S vacancies. *J. Hazard. Mater.*, 2024, 467: 133751.

[172] Kuang, H. N.; He, Z. Y.; Li, M.; Huang, R. F.; Zhang, Y. Q.; Xu, X. M.; Wang, L.; Chen, Y.; Zhao, S. F. Enhancing co-catalysis of MoS_2 for persulfate activation in Fe^{3+}-based advanced oxidation processes *via* defect engineering. *Chem. Eng. J.*, 2021, 417: 127987.

[173] Jiang, Q. B.; Xu, H. F.; Hui, K. S.; Wei, Y. J.; Liu, L. W.; Ye, Z. Q.; Zha, C. Y.; Zheng, M. T.; Lu, J.; Hui, K. N. Inner-layer indium doping achieved highly active and stable sulfur vacancies in MoS_2 for superior sulfur redox kinetics. *Adv. Mater.*, 2025, 37: 2415986.

[174] Zhao, Y. X.; Tang, M. T.; Wu, S. D.; Geng, J.; Han, Z. J.; Chan, K. R.; Gao, P. Q.; Li, H. Rational design of stable sulfur vacancies in molybdenum disulfide for hydrogen evolution. *J. Catal.*, 2020, 382: 320–328.

[175] Su, X. Y.; Guo, Y. X.; Yan, L. G.; Wang, Q. D.; Zhang, W.; Li, X. G.; Song, W.; Li, Y. F.; Liu, G. C. MoS_2 nanosheets vertically aligned on biochar as a robust peroxymonosulfate activator for removal of tetracycline. *Sep. Purif. Technol.*, 2022, 282: 120118.

[176] Chen, Z.; Lian, C.; Huang, K.; Ji, J. H.; Yan, Q. Y.; Zhang, J. L.; Xing, M. Y. "Small amount for multiple times" of H_2O_2 feeding way in MoS_2-Fe_x heterogeneous Fenton for enhancing sulfadiazine degradation. *Chin. Chem. Lett.*, 2022, 33: 1365–1372.

[177] Du, M. M.; Yi, Q. Y.; Ji, J. H.; Zhu, Q. H.; Duan, H.; Xing, M. Y.; Zhang, J. L. Sustainable activation of peroxymonosulfate by the Mo(IV) in MoS_2 for the remediation of aromatic organic pollutants. *Chin. Chem. Lett.*, 2020, 31: 2803–2808.

[178] Huang, L. Z.; Wei, X. L.; Gao, E. L.; Zhang, C. B.; Hu, X. M.; Chen, Y. Q.; Liu, Z. Z.; Finck, N.; Lützenkirchen, J.; Dionysiou, D. D. Single Fe atoms confined in two-dimensional MoS_2 for sulfite activation: A biomimetic approach towards efficient radical generation. *Appl. Catal. B Environ. Energy*, 2020, 268: 118459.

[179] Li, J.; Zhan, G. M.; Yu, Y.; Zhang, L. Z. Superior visible light hydrogen evolution of Janus bilayer junctions *via* atomic-level charge flow steering. *Nat. Commun.*, 2016, 7: 11480.

[180] Qu, S. Y.; Wang, W. H.; Pan, X. Y.; Li, C. L. Improving the Fenton catalytic performance of FeOCl using an electron mediator. *J. Hazard. Mater.*, 2020, 384: 121494.

[181] Zhu, L. L.; Ji, J. H.; Liu, J.; Mine, S.; Matsuoka, M.; Zhang, J. L.; Xing, M. Y. Designing 3D-MoS_2 sponge as excellent cocatalysts in advanced oxidation processes for pollutant control. *Angew. Chem. Int. Ed.*, 2020, 59: 13968–13976.